Neutralization of zoonotic retroviruses by human antibodies: genotype-specific epitopes within the receptor-binding domain from simian foamy virus

Short title: Neutralizing epitopes on zoonotic simian foamy virus envelope

Lasse Toftdal Dynesen[a], Ignacio Fernandez[b], Youna Coquin[a], Manon Delaplace[a], Thomas Montange[a], Richard Njouom[c], Chanceline Bilonga-Ndongo[d], Felix A. Rey[b], Antoine Gessain[a], Marija Backovic[b], and Florence Buseyne[a,*]

[a]Institut Pasteur, Université Paris Cité, CNRS UMR3569, Unité d'Epidémiologie et Physiopathologie des Virus Oncogènes, 75015 Paris, France

[b]Institut Pasteur, Université Paris Cité, CNRS UMR3569, Unité de Virologie Structurale, 75015 Paris, France

[c]Centre Pasteur du Cameroun, Yaoundé, Cameroon

[d]Ministère de la Santé Publique, Yaoundé, Cameroon

[*]corresponding author

Abstract

Infection with viruses of animal origin pose a significant threat to human populations. Simian foamy viruses (SFVs) are frequently transmitted to humans, in which they establish a life-long infection, with the persistence of replication-competent virus. However, zoonotic SFVs do not induce severe disease nor are they transmitted between humans. Thus, SFVs represent a model of zoonotic retroviruses that lead to a chronic infection successfully controlled by the human immune system. We previously showed that infected humans develop potent neutralizing antibodies (nAbs). Within the viral envelope (Env), the surface protein (SU) carries a variable region that defines two genotypes, overlaps with the receptor binding domain (RBD), and is the exclusive target of nAbs. However, its antigenic determinants are not understood. Here, we characterized nAbs present in plasma samples from SFV-infected individuals living in Central Africa. Neutralization assays were carried out in the presence of recombinant SU that compete with SU at the surface of viral vector particles. We defined the regions targeted by the nAbs using mutant SU proteins modified at the glycosylation sites, RBD functional subregions, and genotype-specific sequences that present properties of B-cell epitopes. We observed that nAbs target conformational epitopes. We identified three major epitopic regions: the loops at the apex of the RBD, which likely mediate interactions between Env protomers to form Env trimers, a loop located in the vicinity of the heparan binding site, and a region proximal to the highly conserved glycosylation site N8. We provide information on how nAbs specific for each of the two viral genotypes target different epitopes. Two common immune escape mechanisms, sequence variation and glycan shielding, were not observed. We propose a model according to which the neutralization mechanisms rely on the nAbs to block the Env conformational change and/or interfere with binding to susceptible cells. As the SFV RBD is structurally different from known retroviral RBDs, our data provide fundamental knowledge on the structural basis for the inhibition of viruses by nAbs.

40 ## Introduction

41 Foamy viruses (FVs) are the most ancient of retroviruses [1, 2]. Simian foamy viruses (SFVs) are
42 widespread in nonhuman primates (NHPs), replicate in the buccal cavity, and are transmitted to
43 humans mostly through bites by infected NHPs [2-4]. Such cross-species transmission events currently
44 occur in Asia, Africa, and the Americas. Most individuals known to be infected with zoonotic SFV live
45 in Central Africa, the region at the epicenter of the emergence of HIV-1 and HTLV-1 from their simian
46 reservoirs. In their human hosts, SFVs establish a life-long persistent infection associated with
47 subclinical pathophysiological alterations [5, 6]. Thus far, neither severe disease nor human-to-human
48 transmission have been described, suggesting efficient control of SFV replication and transmission in
49 humans.

50 SFV infection elicits Env-specific neutralizing antibodies (nAbs) that block the entry of viral particles
51 into susceptible cells *in vitro* [7]. Although they do not block cell-to-cell infection *in vitro*, antibodies
52 prevent cell-associated SFV transmission by transfusion in monkeys [8, 9]. SFV Env is cleaved into three
53 subunits, the leader peptide (LP), the surface subunit (SU), which binds to cells, and the
54 transmembrane (TM) subunit, which carries out fusion (Fig. 1). In several SFV species, there are two
55 variants of the *env* gene, defining two genotypes [10-12]. The two variants differ in a discrete region
56 encoding 250 residues, named SUvar, located at the center of the SU and overlapping with most of the
57 receptor-binding domain (RBD) [13]. The RBD is thus bimorphic and we showed that the SUvar region
58 is the exclusive target of genotype-specific nAbs [7].

59 We previously determined the RBD structure at high resolution [14] (Fig. 1A and 1B). The RBDs occupy
60 the space at the top of Env trimer [14, 15] (Fig. 1C). Each RBD has two subdomains. The upper
61 subdomain carries protrusions (loops 1 to 4) that mediate interactions between protomers and the
62 conserved glycosylation site (N8) [14]. The lower subdomain carries the heparan sulfate
63 glycosaminoglycan binding site (HBS) [14]. The RBD has been functionally defined as bipartite [13]. The
64 first essential binding region (RBD1) forms half of the upper subdomain and wraps around the second

65 essential binding region (RBD2) to form the lower subdomain. The central region (called RBDj) is
66 dispensable for cell binding, forms the top of the upper domain, and encompasses loops 3 and 4 (Fig.
67 1D). The genotype-specific SUvar comprises the entire upper RBD subdomain and one third of its lower
68 subdomain, corresponding grossly to the previously defined RBD1.

69 The genotype-specific SUvar region is targeted by nAbs [7] (Fig. 1E). Here, we determined the epitope
70 sites on SUvar recognized by plasma nAbs from SFV-infected African hunters. These individuals were
71 infected by SFV of gorilla origin through bites [3], and we previously described their infecting strains,
72 *ex vivo* blood target cells, antibody response, and medical status [5-7, 9, 11, 16, 17]. We expressed the
73 SFV SU as a soluble recombinant protein that competes with SU present on viral vector particles for
74 binding to plasma nAbs in a neutralization assay. We defined the SUvar regions targeted by the nAbs
75 using mutant SU proteins modified at the glycosylation sites, RBD functional subregions, and genotype-
76 specific sequences that present properties of B-cell epitopes. This immunological study and that on
77 the structure of RBD [14] were carried out concomitantly; thus we integrated structural information
78 as it became available and proposed modes of action for SFV-specific nAbs.

79

80 # Results

81 ## SFV SU recombinant protein competes with the virus for binding to nAbs

82 We sought to define nAb epitopes by performing neutralization assays in the presence of recombinant
83 SU protein that competes with the SU within Env present at the surface of foamy viral vector (FVV)
84 particles. While wildtype (WT) recombinant SU binds to the nAbs, allowing cell infection to proceed,
85 SU mutants with altered nAb epitopes do not (Fig. 2A). We tested several recombinant Env and SU
86 expression constructs, of which the production level and stability varied according to the genotype:
87 Gorilla genotype II (GII) Env-derived constructs were expressed at high levels, whereas gorilla genotype
88 I (GI) Env-derived counterparts were poorly expressed and aggregated (Supplementary Fig. 1 and 2A). To
89 increase the yield and stability of the proteins, we appended the immunoglobulin Fc domain, which
90 acts as a secretion carrier, to the C-terminus of SU. Such chimeric proteins - referred to as
91 immunoadhesins – have been used to produce soluble SFV SU [13]. Nonetheless, the gorilla genotype
92 I (GI) SU immunoadhesin was expressed at insufficient levels. However, we readily produced the
93 chimpanzee genotype I (CI) and GII SU immunoadhesins. We therefore studied epitopes recognized by
94 GII-specific nAbs with the GII immunoadhesin (referred to as ^{GII}SU for the WT sequence) and those
95 recognized by GI-specific nAbs with the CI immunoadhesin (^{CI}SU), as allowed by the frequent cross-
96 neutralization of gorilla and chimpanzee strains belonging to the same genotype [7] and CI and GI
97 SUvar sequence identity of 70% [11].

98 We validated the competition strategy with genotype-matched and mismatched immunoadhesins (Fig.
99 2B, Supplementary Tables 1 and 2, Supplementary Fig. 3). We tested plasma samples from gorilla SFV-
100 infected hunters at the dilution required for 90% reduction of FVV infectivity (IC_{90}) to allow Env-specific
101 antibody saturation by the competitor SU. Thus, plasma samples were tested at the same nAb
102 concentration and responses from different individuals could be compared. We incubated SU with
103 plasma samples before addition to a FVV expressing the matching Env protein and titration of residual
104 infectivity. Both ^{CI}SU and ^{GII}SU blocked the action of nAbs present in genotype-matched plasma

105 samples in a concentration-dependent manner but failed to block the activity of genotype-mismatched
106 samples (Fig. 2B). Importantly, the immunoadhesins did not affect SFV entry (Fig. 2C, [18]), allowing
107 their use as competitors for binding to nAbs in an infectivity assay. The unrelated MLV SU construct
108 (^{MLV}SU) had no impact on either the neutralizing activity of plasma samples or SFV infectivity (Fig. 2B
109 and 2C).

110 We noticed that immunodhesins did not fully block plasma nAbs and hypothesized that this could be
111 due to their monomeric state and lack of the epitopes formed by quaternary structures. In addition,
112 heterogenous glycosylation can lead to partial resistance to neutralization [19-22]. Thus, we evaluated
113 the impact of SU oligomerization and mammalian-type glycosylation on the capacity to block nAbs by
114 testing the following constructs: SU monomers produced in mammalian and insect cells, trimeric Env
115 ectodomains produced in insect cells, and dimers of monomeric SU (i.e., immunoadhesin) produced in
116 mammalian cells. Since all constructs had the same capacity to block the nAbs (Supplementary Fig. 2B),
117 we used the only recombinant proteins available for both genotypes, the SU immunoadhesins.

118 We titrated 11 samples against matched ^{Cl}SU or ^{GII}SU, and one sample from a coinfected individual
119 against both SUs (Supplementary Table 2). The effect of the SU on nAbs can be described by two sample-
120 dependent parameters (Fig. 2D). The first parameter is the affinity, quantified by the protein
121 concentration required to inhibit 50% of the neutralizing activity (IC_{50}). IC_{50} values ranged between 3.3
122 and 12.6 nM for ^{Cl}SU and 2.9 and 12.5 nM for ^{GII}SU, depending on the plasma sample (Fig. 2E). The
123 second parameter is the fraction of neutralizing activity that can be blocked by the SU. Plasma samples
124 contain a polyclonal population of nAbs, some of which bind monomeric SU in its immunoadhesin
125 format, whereas others may not. Taking FVV treated with ^{MLV}SU without plasma as a reference value
126 for full infectivity (100%), ^{Cl}SU and ^{GII}SU restored the infectivity of plasma-treated FVV to between 56%
127 and 94% of infectivity. This value is referred to as maximum infectivity (MaxI) and represents the
128 fraction of nAbs blocked by the SU (Fig. 2D and 2F). We then designed panels of mutant SU proteins

129 (Fig. 2G) and compared their capacity to block nAbs to that of WT SU based on changes in their IC_{50}
130 and MaxI. We first studied GII-specific nAbs using ^{GII}SU before testing GI-specific nAbs using ^{CI}SU.

131 A fraction of nAbs targets glyco-epitopes

132 The GII SUvar domain carries seven of the 11 SU glycosylation sites (Fig. 3A and 3B). We assessed
133 whether these glycans are recognized by nAbs or whether they may shield epitopes from nAb
134 recognition. We produced ^{GII}SU in mammalian cells in the presence of the mannosidase inhibitor
135 kifunensine, which prevents complex-type glycan addition, and treated a fraction with endo-H to
136 remove all glycans. The absence of complex glycans had no impact on nAb blockade by ^{GII}SU (Fig. 3C),
137 in accordance with the data obtained with GII Env constructs expressed in insect cells, which also lack
138 complex glycans (Supplementary Fig. 2). By contrast, the removal of all glycans by Endo-H decreased nAb
139 blockade and protein titration showed lower affinity for the nAbs present in three of four plasma
140 samples (Fig. 3D). We verified that this was not due to aggregation induced by Endo-H treatment
141 (Supplementary Fig. 4). The fact that the removal of glycans did not enhance nAb blockade in the samples
142 tested indicates that the glycans do not shield the majority of nAb epitopes on SFV Env.

143 The N10 glycosylation site is located at different positions for the two genotypes (N422/N423 on GI-
144 D468/CI-PFV strains, N411 on the GII-K74 strain) and we hypothesized that it may be part of a potential
145 epitopic region. The N10 glycosylation knock-down mutant (^{GII}ΔN10) was as efficient as ^{GII}SU in blocking
146 nAbs from all plasma samples (Fig. 3E). N10 belongs to a stretch of seven genotype-specific residues
147 that were replaced by those from the GI-D468 strain. The chimeric protein (^{GII}swap407) blocked nAbs
148 as efficiently as ^{GII}SU for three samples and showed decreased affinity against nAbs for one sample
149 (Fig. 3F). Thus, GII-specific nAbs occasionally target epitopes affected by the N10 glycosylation site.

150 To identify other glycosylation sites targeted by nAbs, we knocked them down one by one, except for
151 N8, which is critical for SU expression [23]. The ^{GII}ΔN7' mutant showed reduced capacity to block nAbs
152 from five of the seven samples (Fig. 3J). ^{GII}ΔN5 and ^{GII}ΔN9 showed reduced capacity to block nAbs from
153 one or two plasma samples (Fig. 3G and 3K). Knock down of N6 and N7 had no impact (Fig. 3H and 3I).

154 Overall, our data indicate that most glycans are not part of epitopes, except those at the N7'
155 glycosylation site.

156 SFV-specific nAbs target the upper RBD subdomain

157 Next, we aimed to locate nAb epitopes on the SU subdomains. On the upper domain, RBDj could be
158 deleted without fully compromising cell binding, whereas the loops it harbors (Fig. 1, 4A and 4B) are
159 essential for infectivity [13, 14]. We therefore constructed a mutant SU with RBDj deleted. ^{GII}ΔRBDj
160 was highly impaired in blocking nAbs from three individuals: the IC_{50} values were above the highest
161 concentration tested (200 nM) and the MaxI values were close to 10%, which is the value of plasma
162 samples incubated with the irrelevant ^{MLV}SU (Fig. 4C). By contrast, ^{GII}ΔRBDj blocked nAbs from the
163 BAD551 plasma sample as efficiently as ^{GII}SU.

164 Among the four loops that emanate from the upper domain L2 (276-281), L3 (416-436), and L4 (446-
165 453) are exposed to solvent and mobile and therefore considered to be candidate epitopic regions
166 [14]. We deleted the loops individually (Fig. 4D-F). ^{GII}ΔL3 blocked all GII-specific samples but one,
167 although with lower affinity. ^{GII}ΔL2 and ^{GII}ΔL4 showed plasma-dependent effects, with three patterns:
168 (1) full activity (such as against BAD551) (2), no or strongly reduced of activity (for example, against
169 BAK133), (3) or a reduced MaxI with unchanged affinity (such as MEBAK88). The last pattern probably
170 reflects the presence of nAbs targeting different epitopes within the same plasma sample, some
171 epitopes being altered on mutant SU, whereas others are not.

172 Before the 3D structure was available, we relied on the insertion of N-linked glycosylation sequences
173 (NXS/T) to disrupt potential epitopes. We selected six genotype-specific sequences predicted to have
174 a disordered secondary structure or to contain a B-cell epitope and built mutant SU with a glycosylation
175 site inserted in the targeted sequence (Supplementary Table 3). Five of the glycosylation sites were
176 inserted in the upper subdomain, with three located within or close to L3 and L4 loops, resulting in
177 decreased affinity against certain plasma nAbs: $^{GII}426_{glyc}$ in L3, $^{GII}450_{glyc}$ in L4, $^{GII}459_{glyc}$ after L4 (Fig. 4G-
178 I). The fourth mutant with reduced affinity against most plasma nAbs, $^{GII}485_{glyc}$, is located in RBDj in

179 the vicinity of N8, which plays a major structural role [14] (Fig. 4J). Finally, $^{GII}263_{glyc}$ had no or only a
180 modest effect on nAb activity, which is consistent with its location at the center of the trimer, which is
181 likely not accessible to antibodies (Fig. 4K, [14]). Overall, glycan insertions confirmed the frequent
182 recognition of RBDj by nAbs.

183 SFV-specific nAbs target epitopes in the lower RBD subdomain

184 In the lower subdomain, the HBS was a candidate epitopic region (Fig. 5). The GII Env ectodomain
185 mutated on HBS residues (^{GII}K342A/R343A or ^{GII}R356A/R369A, [14]) blocked nAbs from three samples
186 as efficiently as their WT counterpart and showed lower affinity for the MEBAK88 plasma sample (Fig.
187 5C and 5D). Thus, nAb activity is modestly affected by mutated HBS residues.

188 In the SU series with glycan insertions in predicted epitopes (Supplementary Table 3), one had a glycan
189 inserted in the lower RBD subdomain ($^{GII}351_{glyc}$) and showed a strongly reduced capacity to block the
190 nAbs (Fig. 5E). The modified residue is located on a solvent-exposed loop (residues 345-353) at the
191 base of the SUvar and is close to the HBS (Fig. 5B). $^{GII}351_{glyc}$ was the first mutant to indicate that nAbs
192 recognize a region of the RBD to which no function has yet been attributed. We therefore focused the
193 following experiments on this novel putative epitope.

194 As $^{GII}351_{glyc}$ was prone to aggregation (Supplementary Fig. 4H), we produced a second batch, half of which
195 was purified by affinity chromatography (standard protocol) and the other half further purified by size
196 exclusion chromatography (SEC) to eliminate the aggregates (Supplementary Fig. 5A). Both $^{GII}351_{glyc}$
197 preparations were unable to block nAbs from the plasma samples (Supplementary Fig. 5B-E). Glycan
198 insertion at an adjacent position in $^{GII}350_{glyc}$ led to the loss of nAb blockade and reduced aggregation
199 (Fig. 5F, Supplementary Fig. 4H). The GII 345-353 loop is one residue shorter than that of the GI-D468
200 and CI-PFV strains (Fig. 5B). The mutant SU with an extra glutamic acid at position 349 ($^{GII}349_{+E}$) showed
201 a strongly reduced capacity to block the nAbs (Fig. 5G). We replaced the seven GII residues by the eight
202 residues from the GI-D468 strain; ^{GII}swap345 showed a reduced ability to block nAbs from five of the
203 seven plasma samples (Fig. 5H). By contrast, swapping the α3-helix located N-terminal to the loop

204 (^{GII}swap333) had no impact on the capacity to block the nAbs (Fig. 5I). Finally, we tested the
205 substitution of residues on the α8-helix facing the 345-353 loop; ^{GII}E502A and ^{GII}L505N showed a
206 reduced capacity to block the nAbs (Fig. 5K and 5K). Overall, these experiments define the 345-353 loop
207 and adjacent α8-helix as a major epitopic region on GII RBD.

208 We directly tested the capacity of plasma nAbs to block the entry of FVVs expressing Env mutated in
209 the 345-353 loop to confirm the data obtained with the competition strategy. We chose to express a
210 mutated Env corresponding to the ^{GII}swap345 mutant, as its cell binding capacity is unaltered in the
211 immunoadhesin format (see below). FVVs with a swapped 345-353 Env loop were produced at the
212 same level as those expressing WT GII-K74 Env and had similar infectious titers and cell binding capacity
213 (Fig. 6A to 6C). We carried out neutralization assays for both vectors using the seven GII-specific plasma
214 samples. In its soluble form, the ^{GII}swap345 protein blocked the neutralizing activity from five plasma
215 samples less efficiently than the ^{GII}SU protein (Fig. 5H). FVVs carrying ^{GII}swap345 SU were less
216 susceptible than those carrying ^{GII}SU to plasma nAbs from three individuals (BAK133, BAK232, BAK228),
217 as reflected by at least two-fold lower neutralization titers against the ^{GII}swap345 carrying vector (Fig.
218 6G to 6I). Plasma samples from individuals BAK55 and MEBAK88 showed similar neutralization titers
219 against both vectors (Fig. 6F and 6J). The ^{GII}swap345 protein blocked nAbs from two plasma samples as
220 efficiently as the ^{GII}SU protein: the sample from individual BAD551 showed similar neutralizing titers
221 against both vectors, whereas the sample from individual BAD447 neutralized the ^{GII}swap345-carrying
222 vector more efficiently than that carrying ^{GII}SU (Fig. 6D and 6E). Thus, despite an imperfect match
223 between the competition assay and direct neutralization data, testing epitope modification in the
224 context of viral particles confirmed that loop 345-353 is recognized by plasma nAbs.

225 GI and GII-specific nAbs target different epitopes

226 We applied a similar strategy using GI-specific plasma samples and ^{CI}SU harboring the mutations with
227 the greatest impact on GII-specific epitopes. We present these data, including a comparison with those
228 obtained with the GII-specific samples (Fig. 7, blue symbols (GI) over light red lines (GII)). GI-specific

229 nAbs targeted glycans removed by Endo-H but not complex glycans and did not recognize N10, for
230 which the location is genotype-specific (Fig. 7A-7C). We could not test the recognition of N7', as it is
231 absent from the CI-PFV strain.

232 The most striking difference between GI and GII epitopes was around residue 350: in sharp contrast to
233 $^{GII}350_{glyc}$ (Fig. 6F), $^{CI}350_{glyc}$ fully blocked GI-specific nAbs (Fig. 7D). In addition, the two chimeric GII SUs
234 with GI residues at positions 333 to 345 and 345 to 351 did not block anti-GI nAbs (Supplementary Fig.
235 6). Neither ^{CI}ΔRBDj nor ^{CI}ΔL3 proteins blocked the nAbs (Fig. 7E and 7G). Thus, L3 is more important for
236 GI- than GII-specific nAbs. Indeed, ^{GII}ΔL3 blocked GII-specific nAbs, although with lower affinity than
237 ^{GII}SU (Fig. 4E). ^{CI}ΔL2 and ^{CI}ΔL4 showed sample-dependent effects, as their GII counterparts (Fig. 7F and
238 7H). $^{CI}463_{glyc}$ blocked GI-specific nAbs, with a reduced MaxI (Fig. 7I), indicating that a fraction of GI-
239 specific nAbs was not blocked, whereas the other was blocked as efficiently as by ^{CI}SU. The
240 corresponding $^{GII}459_{glyc}$ mutant blocked GII-specific nAbs, but with lower affinity than ^{GII}SU (Fig. 4I).
241 Overall, nAbs from GI- and GII-specific plasma samples target different epitopes.

242 The mutations on the SU may have induced local conformational changes with epitope-specific effects
243 or global changes with nonspecific effects. The RBDj deletion had a likely epitope-specific effect on the
244 GII backbone, as ^{GII}ΔRBDj retained its capacity to block one sample containing nAbs that preferentially
245 targeted epitopes outside the RBDj, indicating that a part of the protein was correctly folded (Fig. 4C).
246 However, ^{CI}ΔRBDj and ^{CI}ΔL3 did not display any nAb blocking activity. Thus, we confirmed the results
247 using chimeric SU: ^{GII}swapRBDj (i.e., GI RBDj in ^{GII}SU) blocked nAbs from the four anti-GI plasma samples
248 with a similar or modestly reduced capacity relative to that of ^{CI}SU (Fig. 7J), whereas ^{GII}SU had no
249 blocking activity (Fig. 7K). ^{CI}swapL3 (GII L3 in ^{CI}SU) did not block anti-GI nAbs (Fig. 7L). These data
250 suggest that either GI-specific nAbs recognize the L3 loop.

251 Human plasma samples do not target linear epitopes on SUvar

252 We sought to map additional epitopes by screening plasma samples for binding to synthetic peptides.
253 None of eight plasma samples recognized synthetic peptides spanning loops on the upper domain (Fig.

254 8), indicating that they may be part of conformational epitopes. Furthermore, we screened 17 plasma
255 samples for binding to 37 synthetic peptides spanning the SUvar domain from three viral strains
256 (Supplementary Tables 4 and 5). By ELISA, seven of 17 (41%) plasma samples from SFV-infected individuals
257 reacted against at least one peptide; five locations represented by peptides with GI and/or GII
258 sequences were recognized by at least one plasma sample (Supplementary Fig. 7). Plasma antibodies
259 bound to GI and/or GII peptides irrespective of the SFV genotype against which they were raised.
260 Overall, the peptide binding study showed that most SFV-specific antibodies do not recognize
261 genotype-specific linear epitopes.

262 Genotype-specific residues are involved in SU protein binding to susceptible cells

263 All SU used for epitope mapping were tested for their capacity to bind to human HT1080 cells, which
264 are highly susceptible to gorilla and chimpanzee SFVs [16] (Fig. 9, Supplementary Fig. 8). SU binding was
265 enhanced after glycan removal, possibly through reduced steric hindrance. Deletion of the RBDj
266 reduced binding to susceptible cells, while one-by-one deletion of loops L2, L3, and L4 abolished it. We
267 observed genotype-specific differences; the RBDj deletion had a stronger impact on GII than on CI SU
268 (6- vs. 2.5-fold reduction). Conversely, glycan insertion after L4 had only a moderate impact on the GII
269 SU ($^{GII}459_{glyc}$, 6-fold reduction) but abolished binding of the CI SU ($^{CI}463^{glyc}$, ≈100-fold reduction). In the
270 345-353 loop, glycan insertion strongly affected the binding of GII SU ($^{GII}350_{glyc}$ and $^{GII}351_{glyc}$, ≈50-fold
271 reduction), but there was no effect on ^{CI}SU, mirroring the recognition by the nAbs. Overall, our data
272 support that certain residues involved in cell binding may be genotype-specific.

273 The binding data were also considered in the interpretation of nAb blocking experiments. The mutant
274 SUs that retained their capacity to bind cells were considered to likely be properly folded and loss of
275 nAb blockade could be attributed to the introduced mutation of the epitope. Overall, among all tested
276 mutated immunoadhesins (Supplementary Table 1), only one failed to bind to cells and block the nAbs
277 from all samples tested; thus the related data are not presented.

278 ## Human plasma samples contain nAbs targeting a variable number of epitopic regions

279 Here, we show that nAbs recognize the three solvent-exposed loops on the upper RBD subdomain (Fig.
280 10D). We also identified mutations located C-terminal ($^{GII}459_{glyc}$ and $^{CI}463_{glyc}$) of loop 4 that may affect
281 nAb binding or SU folding. The glycosylation site N7' had the greatest impact on the nAbs. It is located
282 at the opening of the cavity in which the essential N8 glycan is buried [14]. Of note, the glycan inserted
283 in $^{GII}485_{glyc}$ may interfere with N8 function and/or accessibility to nAbs. In the RBD lower subdomain,
284 we show the 345-353 loop to be an immunodominant epitope exclusively recognized by GII-specific
285 nAbs and that it has a role in binding to cells. By contrast, the HBS was not frequently recognized.

286 The effect of the mutant SU on each plasma sample can be summarized as recognition similar to that
287 of WT SU, recognition with a reduced affinity (i.e., increased IC_{50}), blocking a smaller fraction of nAbs
288 than WT SU (i.e., reduced MaxI), or having both effects. This summary highlights the two genotype-
289 specific and immunodominant epitopic regions that we identified: loop 345-353 on ^{GII}SU (Fig. 10B) and
290 L3 on ^{CI}SU (Fig. 10C). Within the RBD apex, four mutant SU correspond to different epitopic sites (L2,
291 L3, L4, and $459/463^{glyc}$). GII-specific plasma samples presented interindividual variations in their
292 specificity. As an example, one sample did not recognize the RBD apex (BAD551), whereas the six other
293 samples did. In addition, samples differed in the number of targeted sites (BAK55 vs. BAK133),
294 Similarly, GI-specific plasma samples contained nAbs focused on a single subdomain (such as BAK55
295 and ^{CI}L3) or target epitopes on up to four sites (BAD348 and BAK132). We tested the recognition of the
296 N8 region by GII-specific samples only and observed that all plasma samples were affected by
297 alteration in the vicinity of N8. We examined the sequence of the identified epitopes and found that
298 all were conserved on the SFV strains infecting individuals from this study or circulating in Central Africa
299 (Supplementary Fig. 9). Overall, we identified three immunodominant epitopic regions (RBD apex, 345-
300 353 loop, and N8 region), of which the sequences are conserved within each genotype. We provide
301 evidence that SFV-infected individuals have nAbs that target several epitopes and recognize epitopes
302 that differ between individuals.

303 ## Discussion

304 Humans infected with zoonotic SFV raised potent neutralizing antibodies that target the genotype-
305 specific SUvar domain overlapping most of the RDB. Here, we aimed to define the sites targeted by
306 these antibodies. We demonstrate that nAbs raised by infected humans recognize three antigenic
307 regions within the SUvar region from genotype II SFV. At least one of these regions is recognized by GI-
308 specific nAbs. Based on the recently solved X-ray structure combined with functional data [13, 14], we
309 hypothesize that the SFV-specific nAbs most likely target sites important for Env trimer formation and
310 conformational changes that lead to membrane fusion, and/or sites important for binding to
311 susceptible cells.

312 We identified only conformational epitopes, despite several attempts to capture linear epitopes using
313 peptides (Fig. 8, Supplementary Fig. 7 and [24]). Our data are consistent with the low reactivity of NHP
314 and human immune sera to denatured Env in immunoblot assays, which contain Abs that bind to native
315 Env in radio-immunoprecipitation and neutralization assays [25-28]. Linear epitopes are usually
316 located in mobile regions of the polypeptide chains. Such mobile segments are absent from the RBD
317 lower subdomain formed by the compact assembly of α-helices and β-sheets [14]. In RBD monomers,
318 the upper subdomain loops appear to be mobile, but inter-protomer interactions probably impose
319 specific conformations in full-length Env. The loops likely form a number of discontinuous epitopes; L2
320 and L4 are in proximity in the monomer and L3 and L4 in the trimer [14].

321 Twelve plasma samples were used in this study, including one from an individual infected by strains
322 belonging to both genotypes. Overall, the epitopic regions were recognized by all or most donors and
323 can be considered to be immunodominant (Fig. 10). Importantly, within each genotype, sequences
324 from the epitopic regions were identical among SFV strains infecting the studied individuals and those
325 circulating in the same geographical area (Supplementary Fig. 9). This observation is consistent with the
326 genetic stability of SFV [29]. The use of polyclonal plasma samples was key to providing a global picture
327 of nAbs raised upon infection with zoonotic SFV, but only epitopes recognized by a significant fraction

328 of plasma antibodies can be detected. Thus, future studies may identify subdominant epitopes and
329 provide a more precise definition of those that are immunodominant.

330 SU proteins fully blocked nAbs from certain samples. However, for most tested samples, the infectivity
331 was maintained but at levels lower than those observed for FVVs not exposed to plasma samples (Fig.
332 2). The heterogeneous glycosylation of the SU could explain the partial blockade of nAbs [27], as
333 proposed for the incomplete neutralization of HIV [19-22]. The SU antigenicity of soluble monomeric
334 proteins probably differed from those contained within viral particles due to the lack of the intra- and
335 interprotomer interactions that form quaternary structures. Thus, our data identify nAb epitopes
336 presented on the monomeric SU domain and indirectly suggest the existence of quaternary epitopes.

337 We have provided experimental evidence for the targeting of different epitopes by nAbs raised after
338 infection by the two SFV genotypes. The RBD fold from different genotypes and FV from different host
339 species is highly conserved [14]. In superinfection-resistance experiments, the CI Env inhibited entry
340 from genotype II strains, indicating that SFV from different genotypes share the use of at least one
341 molecule for entry into target cells; this molecule could act as an attachment factor or receptor [30].
342 The upper RBD subdomain was recognized by both GI- and GII-specific nAbs and the lower RBD
343 subdomain by GII-specific nAbs only. GI-specific nAbs may, nevertheless, recognize epitopes on the
344 lower RBD subdomain that are yet to be identified. Indeed, the biochemical properties of GI Env
345 protein resulted in low expression and protein aggregation. Therefore, we used an SU from
346 chimpanzee genotype I SFV to map epitopes recognized by antibodies induced by a gorilla genotype I
347 SFV. We previously reported that plasma samples cross-neutralize both SFV species, with a strong
348 correlation between nAb titers; however, nAb titers were globally higher against the GI than CI strain
349 [7]. Thus, we may have missed a number of GI-specific epitopes.

350 Relative to other viruses, SFV-specific nAbs target a limited region on Env, i.e., they do not recognize
351 epitopes on the TM nor non-RBD sites of the SU [31-33]. Based on the inhibition mechanisms described
352 for other viruses [33], we can propose a number of possible modes of action. The targeting of RBD

353 loops by nAbs may prevent the fusogenic conformational transition and exposure of the fusion
354 peptide, which is located at the center of the trimer and shielded by the RBD, as visualized on viral
355 particles [15]. It is possible that certain loop-specific nAbs bind several protomers, as described for
356 HIV- and Ebola-specific nAbs [34, 35]. An alternative neutralization mechanism could be the targeting
357 of epitopes located close to the protomer interface, resulting in trimer disruption, as described for HIV-
358 1, SARS-CoV2 and Flu-specific nAbs [36-38].

359 Many nAbs interfere with particle binding to susceptible cells. The existence of a *bona fide* receptor
360 for SFV is yet to be demonstrated. Consequently, the molecular determinants of Env binding to
361 susceptible cells within the lower RBD subdomain are still only roughly defined. Certain nAbs recognize
362 attachment factors, such as an HBS on SARS-CoV2 spike [39]. The SFV Env mutants deficient for HS
363 binding efficiently blocked most plasma samples, indicating that HBS is either not a major nAb target
364 or that the antigenicity of these mutants is preserved. Of note, the N7' site located in the vicinity of
365 HBS was recognized. All SU designed to map potential B-cell epitopes were tested for their capacity to
366 bind susceptible cells. SU from the two genotypes differed in certain residues involved in cell binding.
367 Most notably, nAbs recognizing the 345-353 loop may prevent GII Env binding, whereas the loop on GI
368 Env is not involved in cell binding and is not targeted by nAbs (Fig. 9). This last observation highlights,
369 for the first time, genotype-specific differences in SFV binding to susceptible cells and could be a
370 starting point for further studies on identifying attachment factors and receptors for SFV.

371 Our choice of a functional strategy to map the epitopes targeted by nAbs proved to be critical due to
372 the lack of linear epitopes. Overall, the use of human samples and soluble SU as competitor allowed
373 us to create the first map of targeted regions. We considered several caveats (polyspecificity of plasma
374 samples, absence of quaternary epitopes). We also carefully considered the possible nonspecific effect
375 of mutations on protein folding, which could generate misleading results. Certain mutants were,
376 indeed, poorly expressed and could not be used (Supplementary Table 1). A number of these limitations

377 may be overcome in the future with the use of alternative tools, such as human monoclonal antibodies
378 and subviral particles.

379 Human infection with zoonotic SFV represents a model for cross-species transmission of retroviruses
380 leading to persistent infection that is successfully controlled by the immune system. We have
381 previously reported the presence of potent nAbs in most infected individuals [24]. Here, we have
382 mapped major antigenic sites. Concerning the control of SFV in humans, a notable result from the
383 present study is that two immune escape mechanisms, sequence variation and glycan shielding, were
384 not observed. The SFV RBD is structurally different from known and modelled retroviral RBDs [40]. We
385 have provided a novel model integrating structural, genetic, functional, and immunological knowledge
386 on the bimorphic SFV RBD. We have thus gained information on the two SFV genotypes that have
387 persisted for over 30 million years of evolution with their animal hosts. Through the study of SFV and
388 its unique properties, we should also gain fundamental knowledge on the structural basis for the
389 inhibition of viruses by nAbs.

390

391 # Methods

392 ## Human plasma samples

393 Blood samples were drawn from adult populations living in villages and settlements throughout the
394 rainforests of Cameroon. Participants gave written informed consent. Ethics approval was obtained
395 from the relevant national authorities in Cameroon (the Ministry of Health and the National Ethics
396 Committee) and France (Commission Nationale de l'Informatique et des Libertés, Comité de Protection
397 des Personnes Ile de France IV). The study was registered at www.clinicaltrials.gov,
398 https://clinicaltrials.gov/ct2/show/NCT03225794/. SFV infection was diagnosed by a clearly positive
399 Gag doublet on Western blots using plasma samples from the participants and the amplification of the
400 integrase gene and/or LTR DNA fragments by PCR using cellular DNA isolated from blood buffy-coats
401 [3]. We identified the SFV origin by phylogenetic analysis of the integrase gene sequence [3]. The SFV
402 genotype was determined by amplification of the SUvar DNA fragment by PCR [7]. Plasma samples
403 from 24 participants were used for this study (Supplementary Tables 2 and 4). Four participants were not
404 infected with SFV and 20 were infected with a gorilla SFV.

405 ## Viral strains, amino-acid numbering, and Env domain nomenclature

406 We used sequences from primary zoonotic gorilla SFVs, SFVggo_huBAD468 (GI-D468, JQ867465) and
407 SFVggo_huBAK74 (GII-K74, JQ867464) [41] and the laboratory-adapted chimpanzee SFV,
408 SFVpsc_huPFV (CI-PFV, KX087159) [42] for the synthesis of foamy viral vectors (FVV) and envelope
409 proteins and peptides. For simple reference to previously described Env sequences and functions, we
410 used the amino-acid positions from the CI-PFV strain, unless otherwise stated. The GI-D468, GII-K74,
411 and CI-PFV sequence alignment are shown in supplementary Fig. 1. When referring to infecting SFV
412 strains and the antibodies raised against them, gorilla and chimpanzee genotype I SFV are referred to
413 as GI and CI, respectively; gorilla genotype II SFV is referred to as GII.

414 ## Cells

415 Baby hamster kidney (BHK)-21 cells (ATCC-CLL-10, hamster kidney fibroblast) were cultured in DMEM-
416 5% fetal bovine serum (FBS). HT1080 cells (ECACC 85111505, human fibrosarcoma) were cultured in
417 Eagle's Minimum Essential Medium with Earle's Balanced Salts and L-glutamine supplemented with
418 10% FBS and 1% L-glutamine. Human embryonic kidney 293T cells (Cat. N° 12022001, Sigma) were
419 cultured in DMEM-10% FBS. FreeStyle 293-F cells (Life Technologies) were cultured in Ex-cell 293 HEK
420 serum-free medium supplemented with 5 µg/mL phenol red sodium salt, 2% L-glutamine, and 0.2x
421 penicillin-streptomycin.

422 ## Plasmids

423 The four-component CI-PFV FVV system (pcoPG, pcoPP, pcoPE, and puc2MD9) and the gorilla SFV Env
424 constructs containing sequence from the zoonotic GI-D468 and GII-K74 *env* genes have already been
425 described [7, 43]. Novel plasmids were synthesized by Genscript (Piscataway, NJ, USA). We built a FVV
426 expressing β-galactosidase with a nuclear localization signal (puc2MD9-B-GAL) by replacement of the
427 *gfp* gene in the puc2MD9 backbone for easier image analysis on our quantification device. GII-K74 Env
428 with swapped 345-353 loop was constructed with the boundaries used for SU (Supplementary Table 1).

429 Immunoadhesin constructs express a fusion protein formed by the murine IgK signal peptide, SFV SU
430 with deleted furin cleavage site (aa 127-567), and the heavy chain (hinge-CH2-CH3) of murine IgG2a.
431 A Twin-Strep-tag was fused after the mIgG2a to facilitate immunoadhesin purification, except for the
432 first immunoadhesin constructs (^{GII}ΔRBDj, ^{GII}swapRBDj and ^{GII}ΔN10). The murine leukemia virus (MLV)
433 gp70 SU (aa 34-475, strain FB29, NP_040334.1) was fused to the Twin-Strep-tag. All genes were codon
434 optimized for expression in mammalian cells and placed under the control of a CMV promotor and
435 intron in the pcZI plasmid [44].

436 The codon-optimized synthetic genes encoding GII-K74 SU (aa 127-566) and ectodomain (aa 91-907,
437 [14]) were cloned into the already described pT350 plasmid [45], which contains the *Drosophila*
438 metallothionein promoter, which is inducible by divalent cations [46], the *Drosophila* BiP signal peptide

439 (MKLCILLAVVAFVGLSLG) at the N-terminus and a Twin-Strep-tag
440 (AGWSHPQFEKGGGSGGGSGGGSWSHPQFEK) for affinity purification at the C-terminus. Stable S2 cell
441 lines were generated by antibiotic resistance and protein production was induced by the addition of 2
442 µM $CaCl_2$. For expression in mammalian cells, the murine IgK signal peptide was fused at the N-
443 terminus of codon-optimized genes encoding GII-K74 SU (aa 127-566). The genes were placed under
444 the control of the CMV promoter and intron [44] by insertion into the pcDNA3.1 vector. The
445 ectodomain proteins with mutation in HBS are described in [14].

446 Protein expression and purification

447 293-F cells were seeded at 2.5 10^6 cells/mL in FreeStyle 293 Expression medium and transfected by the
448 addition of plasmid DNA (2 µg/mL) and LipoD293 (6 µg/mL #SL100668, Tebu-bio). After 24 h, cells were
449 diluted 1:1 in Ex-cell culture media and cultivated for another 48 h and the supernatants collected and
450 stored at -80°C. For the expression of immunoadhesins with high-mannose-type glycans, transfected
451 cells were cultivated in the presence of 5 µM Kifunensine mannosidase inhibitor (#BML-S114-0005,
452 Enzo Life Sciences). Glycans were removed by incubating the immunoadhesins ON at room
453 temperature (RT) with endoglycosidase H (endo-H, 0.8 U/mL, #P0702L, New England Biolabs) in 50
454 mM Na acetate-50 mM NaCl, pH 6. Supernatants were thawed and filtrated through a 0.2 µm filter
455 before centrifugation at 4500 x g at 4°C in VivaSpin tubes (Sartorius). The first-generation
456 immunoadhesins do not carry the Twin-Strep-tag and were purified using Protein A Mag Sepharose™
457 Xtra beads (50 µL beads/mL of supernatant; #28-9670-62, GE Healthcare) using binding buffer pH 7,
458 0.2 M Na_3PO_4 (#28-9030-59, Ab Buffer Kit, GE Healthcare). Beads were incubated at 4°C on a rotator
459 ON. Proteins were eluted with a pH 2.5 elution buffer containing 0.2 M Glycine-HCl and neutralized
460 with 1 M Tris-HCl, pH 9 (#PUR004, NEO Biotech, CliniSciencesProteus). Immunoadhesins and ^{MLV}SU
461 fused to Twin-Strep-tag were purified using Gravity Flow Strep-Tactin XT Superflow High-Capacity
462 columns (#2-4031-001, Iba Lifescience). Concentrated proteins were resuspended in buffer W at pH 8
463 and incubated with BioLock (#2-0205-050, Iba Life sciences) for 15 min at RT to neutralize biotin.
464 Loading onto the columns and elution were performed according to manufacturer's instructions.

465 GII-K74 SU, WT, and mutated ectodomains were expressed in *Drosophila* Schneider's cell line 2 (S2)
466 cells following the standard protocol [47]. GII monomeric SU and trimeric ectodomain proteins were
467 purified by affinity chromatography on a Strep-Tactin column (IBA Biosciences), followed by size-
468 exclusion chromatography on Superdex 200, using standard methods provided by the manufacturers.

469 Protein concentrations were measured by NanoDrop. To verify protein purity and aggregate
470 formation, 1.5 µg of purified proteins was heat-denaturated at 70°C for 10 min in NuPAGE LDS sample
471 buffer (#NP0007, Introgen), with or without NuPAGE reducing buffer (50 mM DTT; #NP0009,
472 Invitrogen). Samples were loaded onto a precast NuPAGE 4-12% Bis-Tris gel (#NP0322, Invitrogen). The
473 gel was incubated with Bio-Safe Coomassie staining solution (#1610786, Bio-Rad) for 2 h with gentle
474 shaking, rinsed in H_2O ON, and imaged using a G:BOX (Syngene) (Supplementary Fig. 4).

475 Western blots

476 Western-blot analysis of protein expression was performed on cell supernatants. Samples were heat-
477 denaturated and reduced as described for purified proteins before loading onto precast NuPAGE 4-
478 12% Bis-Tris gels (#NP0322, Invitrogen). Proteins were migrated for 2-3 h at 120 V in NuPAGE MOPS
479 SDS running buffer (#NP0001, Invitrogen) and transferred onto a PVDF membrane (#1704156, Bio-Rad)
480 using a Trans-Blot Turbo transfer system (Bio-Rad). Membranes were blocked and antibody labeled in
481 Tris-buffered saline (TBS)-0.1%Tween-5% BSA. For Strep-tag detection, membranes were incubated
482 with StrepMAB-Classic monoclonal antibody conjugated to HRP (0.05 µg/mL, #2-1509-001, Iba
483 Lifesciences) for 2 h at RT. For SFV SU detection, membranes were incubated with a biotinylated anti-
484 SU murine antibody ON at 4°C (3E10, 1 µg/mL), washed three times in TBS-0.1% Tween for 10 min and
485 incubated with Streptavidin-HRP (1:2000, #DY998, Biotechne). Membranes were washed three times
486 in TBS-0.1% Tween for 10 min before revelation with SuperSignal West Pico PLUS chemiluminescence
487 substrate (#34579, ThermoFischer Scientific) and signal acquisition using a G:BOX.

488 ## Foamy viral vectors (FVVs)

489 FVV particles were produced by co-transfection of HEK293T cells by the four plasmids. Fifteen μg total
490 DNA (gag:env:pol:transgene ratio of 8:2:3:32) and 45 μl polyethyleneimine (#101-10N, JetPEI,
491 Polyplus) were added to a 10 cm^2 culture dish seeded with 4 x 10^6 293T cells. Supernatants were
492 collected 48 h post-transfection, clarified at 500 x g for 10 min, filtered using a 0.45 μm filter, and
493 stored as single-use aliquots at -80°C. FVVs were titrated as described [7, 48], with minor modifications
494 to optimize X-Gal staining of transduced cells, which was lighter than that of infected cells. Briefly, FVV
495 samples were thawed and clarified by spinning at 10,000 x g at 4°C for 10 min. Serial five-fold dilutions
496 were added in triplicate to sub-confluent BHK-21 cells seeded in 96-well plates and cultured for 72 h
497 at 37°C. Plates were fixed with 0.5% glutaraldehyde in PBS for 10 min at RT, washed with PBS, and
498 stained with 150 μl X-gal solution containing 2 mM $MgCl_2$, 10 mM potassium ferricyanide, 10 mM
499 potassium ferrocyanide, and 0.8 mg/mL 5-bromo-4-chloro-3-indolyl-B-D-galactopyranoside in PBS for
500 3 h at 37°C. Blue-stained cells were counted using an S6 Ultimate Image UV analyzer (CTL Europe,
501 Bonn, Germany). One infectious unit was defined as one blue cell. Cell transduction by FVV is a
502 surrogate for viral infectivity and FVV titers are expressed as infectious units (IU)/mL.

503 The yield of FVV particles was estimated by quantifying particle-associated transgene RNA. FVV RNA
504 was extracted from raw cell supernatants using a QIAamp Viral RNA Extraction Kit (Qiagen), treated
505 with a DNA-free kit (Life Technologies), and retro-transcribed with Maxima H Minus Reverse
506 Transcriptase (Thermo Fischer Scientific) using random primers (Thermo Fischer Scientific) according
507 to the manufacturers' instructions. qPCR was performed on cDNA using BGAL primers (BGAL_F 5'
508 AAACTCGCAAGCCGACTGAT 3' and BGAL_R 5' ATATCGCGGCTCAGTTCGAG 3') with a 10-min
509 denaturation step at 95°C and 40 amplification cycles (15 s at 95°C, 20 s at 60°C, and 30 s at 72°C)
510 carried out using an Eppendorf realplex2 Mastercycler (Eppendorf). A standard curve prepared with
511 serial dilutions of puc2MD9-BGAL plasmid was used to determine the FVV copy number. Results are
512 expressed as vector particles/mL, considering that each particle carries two copies of the transgene.

513 To test the capacity of mutated Env to mediate the binding of vector particles to cells, HT1080 cells
514 were incubated with the FVV particles (1, 10 and 100 particles/cell) on ice for 1 h. The cells were
515 washed three times with PBS to eliminate unbound FVV and RNA was extracted using an RNeasy plus
516 mini-Kit (Qiagen) according to manufacturer's protocol and RT performed as described for FVV RNA
517 quantification. Bound FVV was quantified by qPCR of the *bgal* gene as described for vector titration;
518 cells were quantified by qPCR amplification of the *hgapdh* gene with the following primers: hGAPDH_F
519 5' GGAGCGAGATCCCTCCAAAAT 3' and hGAPDH_R 5' GGCTGTTGTCATACTTCTCATGG 3'. The qPCR
520 reaction conditions were the same as those used to amplify the *bgal* gene. The relative mRNA
521 expression of *bgal* versus *hgapdh* was calculated using the -ΔΔCt method, and relative binding as 2-
522 ΔΔCt.

523 ## Neutralization assays

524 Prior to use in neutralization assays, plasma samples were diluted 1:10 in DMEM + 1 mM $MgCl_2$,
525 decomplemented by heating at 56°C for 30 min, and frozen at -80°C as single-use aliquots. Thawed
526 plasma samples were clarified by spinning at 10,000 x g for 10 min at 4°C. Serial two-fold dilutions were
527 incubated with FVV for 1 h at 37°C before titration in triplicate and residual infectivity quantified using
528 the 96-well plate microtitration assay described above. P96-well plates seeded with 5,000 BHK-21 cells
529 were exposed to 300 IUs of FVV. Neutralization titers were defined as the inverse of the plasma dilution
530 required to reduce viral infectivity by half. Plasma samples were initially titrated against replicating
531 virus [7]. We selected those with neutralization titers > 1:100 against the virus and performed plasma
532 titration against the FVV. We defined the plasma dilution required for a 90% reduction of FVV
533 infectivity and used it as the fixed concentration for the nAbs. Plasma samples were incubated with
534 serial dilutions of recombinant Env proteins for 1 h at 37°C. FVV was then mixed with the
535 plasma/protein preparation and incubated 1 h at 37°C before addition to BHK-21 cells. FVV infectivity
536 was quantified 72 h later as described for their titration. All conditions were tested in triplicate and the
537 mean IU/well calculated. Cells transduced with mock treated FVV (i.e., incubated with ^{MLV}SU at 20 nM
538 or with medium) were quantified on each plate and this value used as a reference. Relative infectivity

539 was calculated for wells treated with the plasma/protein mix and is expressed as the percentage of the
540 reference value. The WT SU (^{GII}SU or ^{CI}SU) matched with the FVV Env was titrated along with the tested
541 mutant SU on every plate in every experiment for each plasma tested. All SU were tested against each
542 plasma at least twice and against at least four plasma samples. In the first assay (screening), SU were
543 added at three concentrations, ranging from 200 to 2 nM. In the second assay (confirmation), SU with
544 activity similar to that of WT or with no activity were tested a second time at three dilutions. Mutant
545 SU with intermediate activity were titrated in a three-fold serial dilution setting starting at 60 nM. We
546 used two parameters to define the action of the SU on the nAbs from each plasma sample: maximum
547 infectivity (MaxI) and 50% inhibitory concentration (IC_{50}). MaxI corresponds to the maximal infectivity
548 in the presence of SU-blocking nAbs and is defined as the mean relative infectivity at the two highest
549 doses tested. The IC_{50} values were calculated by plotting the relative infectivity as a function of SU
550 concentration and a four parameters regression modeling of the Prism software (Version 9, GraphPad).
551 Mutant SU with nAb activity similar to the WT one were given its IC_{50}, and those with minimal or no
552 activity were given an arbitrary IC_{50} value of 200 nM, corresponding to the highest concentration of SU
553 tested.

554 ## SFV Env binding to cells

555 SU were thawed at RT and clarified at 10,000 x g for 10 min. HT1080 cells were treated with trypsin-
556 EDTA and 5 x 10^5 cells resuspended in 0.1 mL FACS buffer (PBS-0.1% BSA) containing the SU and
557 incubated on ice for 1 h. Cells were washed twice and incubated with donkey anti-murine IgG-(H+L)-
558 AF488 (20 µg/mL, #A21202, Invitrogen) on ice for 30 min. Cells were washed and resuspended in 0.2
559 mL PBS-2% PFA. Data were acquired on a CytoFlex cytometer (Beckman Coulter) and analyzed using
560 Kaluza software. A minimum of 25,000 cells were acquired. Single cells were selected by sequential
561 gating on FSC-A/SSC-A and SSC-A/SSC-H dot-plots (Supplementary Fig. 8). SU binding is expressed as the
562 ratio of mean fluorescence intensity (MFI) of SU-treated over untreated cells. Each SU was tested twice
563 at 3, 30, and 300 nM. The MFI ratios were plotted as a function of SU concentration and the area under

564 the curve was calculated (Supplementary Fig. 8). To limit inter-experimental variation, WT SU were
565 included in every experiment and the binding level of mutant SU normalized to that of the WT.

566 Peptides

567 The SUvar (aa 248-488) sequences from the GI-D468 and GII-K74 strains were analyzed using linear B-
568 cell epitope prediction software available on the Immune Epitope Data Base
569 (http://tools.iedb.org/bcell/), which are based on known B-cell epitopes (LBtope [49]), hydrophilicity
570 (Parker prediction replaced by Bepipred software [50]), and protrusion outside of globular proteins
571 (Ellipro [51]). In addition, we manually inspected viral sequences for stretches of genotype-specific
572 epitopes. We selected 14 sequences and tested the corresponding GI-D468 and GII-K74 peptides, as
573 well as nine CI-PFV peptides from a previously synthesized peptide set [24] (Supplementary Table 5). After
574 resolution of the RBD crystal structure, we designed a second peptide set corresponding to the four
575 loops located in the RBD upper subdomain [14]. As positive controls, we used the N_{96}-V_{110}
576 (NKDIQVLGPVIDWNV from SFV Env LP) and I_{176}-I_{199} (INTEPSQLPPTAPPLLPHSNLDHI from HTLV-1 gp46)
577 peptides containing immunodominant epitopes [24]. Peptides were synthesized by Smartox SAS
578 (Saint-Martin d'Hères, France) or Genscript (Leiden, The Netherlands) and were tested individually.

579 ELISA

580 The protocol was described in [24]. Briefly, peptides diluted in carbonate buffer at 1 µg/mL were
581 coated on clear high-binding polystyrene 96-well microplates (Biotechne) overnight (ON) at +4°C.
582 Plasma samples were diluted at 1:200 in phosphate buffered saline (PBS)-0.1% bovine serum albumin
583 (BSA)-0.1% Tween20. Bound plasma antibodies were detected with horseradish peroxidase (HRP)-
584 conjugated goat anti-human IgG H+L (0.02 µg/mL, #109-035-008, Jackson Immuno Research Europe).
585 The peptide diluent was used as the negative control and antibody binding to peptides is expressed as
586 the difference in OD ($\Delta_{OD} = OD_{test} - OD_{control}$). Plasma samples from three SFV-uninfected individuals
587 were tested for binding to the 37 peptides. The mean + 2 SD of Δ_{OD} (0.14) was used to define the

588 positivity cutoff. The proportion of responding individuals was calculated among those infected with a
589 given virus (SFV, n = 17; HTLV-1, n = 7).

590 Statistical analysis

591 Mutations in the SU modified their ability to block the nAbs in two ways: either by reducing avidity,
592 leading to a higher IC_{50}, or by the fraction of plasma nAbs blocked, leading to lower maximal infectivity.
593 For each plasma sample, the IC_{50} and MaxI were tested for the WT SU in at least five experiments. The
594 threshold value defining a statistically significant change relative to WT was defined as the mean +
595 3*SD for the IC_{50} and the mean - 3*SD for MaxI. Thresholds were defined for each plasma sample. The
596 infectious titers, particle concentration, percentage of infectious particles, and quantity of bound FVV
597 carrying WT and mutant SU were compared using the paired t test (GraphPad Prism 9 software).

598

Acknowledgements

We thank H. Mouquet and V. Lorin for sharing the 293-F cells and advice. We are grateful to Mathilde Couteaudier for mentoring MD and LTD in their performance of the experimental work. We used devices from the Cytometry and Biomarker Utechs at the Institut Pasteur and we thank their staff for their support and advice. We thank Delphine Brun from the Unité de Virologie Structurale for technical assistance. The manuscript has been edited by a native English speaker.

Funding

This work was supported by the Agence Nationale de la Recherche (ANR-10-LABX62-IBEID, Intra-Labex Grant (MB)), and the Programme de Recherche Transversal from the Institut Pasteur (PTR2020-353 ZOOFOAMENV, FB). SFV protein production was supported by the European Virus Archive-GLOBAL project, which has received funding from the EU Horizon 2020 Research and Innovation Programme (grant agreement number 871029). LTD was supported by the Pasteur-Paris-University (PPU) International Doctoral Program and the Fondation pour la Recherche Médicale, including additional supportive funding from the Danish Pasteur Society, Augustinus Fonden, Knud-Højgaards Fond, and Viet-Jacobsen Fonden. The funding agencies had no role in the study design, generation of results, or writing of the manuscript.

Authors contribution

FB, MB, FR, and AG designed the project. FB and MB supervised the project and acquired funding. LTD, IF, YC, MD, and TM performed the experiments. LTD, IF, FB, and MB analyzed the data. AG, RN, and CBN collected the human samples. LTD and YC provided figures and text elements for the draft. FB wrote the initial and final drafts. All authors participated in reviewing the drafts.

620 # References

621 1. Rethwilm A, Bodem J. Evolution of foamy viruses: the most ancient of all retroviruses. Viruses.
622 2013;5:2349-74.
623 2. Pinto-Santini DM, Stenbak CR, Linial ML. Foamy virus zoonotic infections. Retrovirology.
624 2017;14:55.
625 3. Betsem E, Rua R, Tortevoye P, Froment A, Gessain A. Frequent and recent human acquisition
626 of simian foamy viruses through apes' bites in Central Africa. PLoS Pathog. 2011;7:e1002306.
627 4. Filippone C, Betsem E, Tortevoye P, Cassar O, Bassot S, Froment A, et al. A severe bite from a
628 nonhuman primate is a major risk factor for HTLV-1 infection in hunters from Central Africa. Clin Infect
629 Dis. 2015;60:1667-76.
630 5. Buseyne F, Betsem E, Montange T, Njouom R, Bilounga Ndongo C, Hermine O, et al. Clinical
631 signs and blood test results among humans infected with zoonotic simian foamy virus: a case-control
632 study. J Infect Dis. 2018;218:144-51.
633 6. Gessain A, Montange T, Betsem E, Bilounga Ndongo C, Njouom R, Buseyne F. Case-control
634 study of immune status in humans infected with zoonotic gorilla simian foamy viruses. J Infect Dis.
635 2020;221:1724-33.
636 7. Lambert C, Couteaudier M, Gouzil J, Richard L, Montange T, Betsem E, et al. Potent neutralizing
637 antibodies in humans infected with zoonotic simian foamy viruses target conserved epitopes located
638 in the dimorphic domain of the surface envelope protein. PLoS Pathog. 2018;14:e1007293.
639 8. Williams DK, Khan AS. Role of neutralizing antibodies in controlling simian foamy virus
640 transmission and infection. Transfusion. 2010;50:200-7.
641 9. Couteaudier M, Montange T, Njouom R, Bilounga-Ndongo C, Gessain A, Buseyne F. Plasma
642 antibodies from humans infected with zoonotic simian foamy virus do not inhibit cell-to-cell
643 transmission of the virus despite binding to the surface of infected cells. PLoS Pathog.
644 2022;18:e1010470.
645 10. Galvin TA, Ahmed IA, Shahabuddin M, Bryan T, Khan AS. Identification of recombination in the
646 envelope gene of simian foamy virus serotype 2 isolated from Macaca cyclopis. J Virol. 2013;87:8792-
647 7.
648 11. Richard L, Rua R, Betsem E, Mouinga-Ondeme A, Kazanji M, Leroy E, et al. Cocirculation of two
649 *env* molecular variants, of possible recombinant origin, in gorilla and chimpanzee simian foamy virus
650 strains from Central Africa. J Virol. 2015;89:12480-91.
651 12. Aiewsakun P, Richard L, Gessain A, Mouinga-Ondémé A, Afonso PV, Katzourakis A. Modular
652 nature of simian foamy virus genomes and their evolutionary history. Virus Evol. 2019;5:vez032.
653 13. Duda A, Luftenegger D, Pietschmann T, Lindemann D. Characterization of the prototype foamy
654 virus envelope glycoprotein receptor-binding domain. J Virol. 2006;80:8158-67.
655 14. Fernandez I, Dynesen LT, Coquin Y, Pederzoli R, Brun D, Haouz A, et al. The crystal structure of
656 a simian Foamy Virus receptor binding domain provides clues on the entry to host cells. In revision,
657 Nature Comm.;https://www.biorxiv.org/content/10.1101/2022.10.04.509876v1.
658 15. Effantin G, Estrozi LF, Aschman N, Renesto P, Stanke N, Lindemann D, et al. Cryo-electron
659 microscopy structure of the native prototype foamy virus glycoprotein and virus architecture. PLoS
660 Pathog. 2016;12:e1005721.
661 16. Couteaudier M, Calzada-Fraile D, Montange T, Gessain A, Buseyne F. Inhibitors of the
662 interferon response increase the replication of gorilla simian foamy viruses. Virology. 2020;541:25-31.
663 17. Rua R, Betsem E, Montange T, Buseyne F, Gessain A. *In vivo* cellular tropism of gorilla simian
664 foamy virus in blood of infected humans. J Virol. 2014;88:13429-35.
665 18. Berg A, Pietschmann T, Rethwilm A, Lindemann D. Determinants of foamy virus envelope
666 glycoprotein mediated resistance to superinfection. Virology. 2003;314:243-52.
667 19. McCoy LE, Falkowska E, Doores KJ, Le K, Sok D, van Gils MJ, et al. Incomplete neutralization
668 and deviation from sigmoidal neutralization curves for HIV broadly neutralizing monoclonal antibodies.
669 PLoS Pathog. 2015;11:e1005110.

670 20. Doores KJ, Burton DR. Variable loop glycan dependency of the broad and potent HIV-1-
671 neutralizing antibodies PG9 and PG16. J Virol. 2010;84:10510-21.
672 21. Kim AS, Leaman DP, Zwick MB. Antibody to gp41 MPER alters functional properties of HIV-1
673 Env without complete neutralization. PLoS Pathog. 2014;10:e1004271.
674 22. Prasad VM, Leaman DP, Lovendahl KN, Croft JT, Benhaim MA, Hodge EA, et al. Cryo-ET of Env
675 on intact HIV virions reveals structural variation and positioning on the Gag lattice. Cell. 2022;185:641-
676 53.
677 23. Luftenegger D, Picard-Maureau M, Stanke N, Rethwilm A, Lindemann D. Analysis and function
678 of prototype foamy virus envelope N glycosylation. J Virol. 2005;79:7664-72.
679 24. Lambert C, Batalie D, Montange T, Betsem E, Mouinga-Ondeme A, Njouom R, et al. An
680 immunodominant and conserved B-cell epitope in the envelope of simian foamy virus recognized by
681 humans infected with zoonotic strains from apes. J Virol. 2019;93:e00068-19.
682 25. Netzer KO, Rethwilm A, Maurer B, Termeulen V. Identification of the major immunogenic
683 structural proteins of human foamy virus. J Gen Virol. 1990;71:1237-41.
684 26. Hahn H, Baunach G, Brautigam S, Mergia A, Neumannhaefelin D, Daniel MD, et al. Reactivity
685 of primate sera to foamy virus Gag and Bet proteins. J Gen Virol. 1994;75:2635-44.
686 27. Herchenroder O, Moosmayer D, Bock M, Pietschmann T, Rethwilm A, Bieniasz PD, et al. Specific
687 binding of recombinant foamy virus envelope protein to host cells correlates with susceptibility to
688 infection. Virology. 1999;255:228-36.
689 28. Cummins JE, Boneva RS, Switzer WM, Christensen LL, Sandstrom P, Heneine W, et al. Mucosal
690 and systemic antibody responses in humans infected with simian foamy virus. J Virol. 2005;79:13186-
691 9.
692 29. Switzer WM, Salemi M, Shanmugam V, Gao F, Cong ME, Kuiken C, et al. Ancient co-speciation
693 of simian foamy viruses and primates. Nature. 2005;434:376-80.
694 30. Hill CL, Bieniasz PD, McClure MO. Properties of human foamy virus relevant to its development
695 as a vector for gene therapy. J Gen Virol. 1999;80:2003-9.
696 31. Burkhart MD, Kayman SC, He YX, Pinter A. Distinct mechanisms of neutralization by
697 monoclonal antibodies specific for sites in the N-terminal or C-terminal domain of murine leukemia
698 virus SU. J Virol. 2003;77:3993-4003.
699 32. Chuang GY, Zhou J, Acharya P, Rawi R, Shen CH, Sheng Z, et al. Structural survey of broadly
700 neutralizing antibodies targeting the HIV-1 Env trimer delineates epitope categories and characteristics
701 of recognition. Structure. 2019;27:196-206.e6.
702 33. Murin CD, Wilson IA, Ward AB. Antibody responses to viral infections: a structural perspective
703 across three different enveloped viruses. Nature Microbiol 2019;4:734-47.
704 34. McLellan JS, Pancera M, Carrico C, Gorman J, Julien JP, Khayat R, et al. Structure of HIV-1 gp120
705 V1/V2 domain with broadly neutralizing antibody PG9. Nature. 2011;480:336-U86.
706 35. Milligan JC, Davis CW, Yu X, Ilinykh PA, Huang K, Halfmann PJ, et al. Asymmetric and non-
707 stoichiometric glycoprotein recognition by two distinct antibodies results in broad protection against
708 ebolaviruses. Cell. 2022;185:995-1007.e18.
709 36. Bangaru S, Lang S, Schotsaert M, Vanderven HA, Zhu X, Kose N, et al. A site of vulnerability on
710 the Influenza virus hemagglutinin head domain trimer interface. Cell. 2019;177:1136-52.e18.
711 37. Wrobel AG, Benton DJ, Hussain S, Harvey R, Martin SR, Roustan C, et al. Antibody-mediated
712 disruption of the SARS-CoV-2 spike glycoprotein. Nat Comm. 2020;11:5337.
713 38. Turner HL, Andrabi R, Cottrell CA, Richey ST, Song G, Callaghan S, et al. Disassembly of HIV
714 envelope glycoprotein trimer immunogens is driven by antibodies elicited via immunization. Science
715 Adv. 2021;7:eabh2791.
716 39. Bermejo-Jambrina M, Eder J, Kaptein TM, van Hamme JL, Helgers LC, Vlaming KE, et al.
717 Infection and transmission of SARS-CoV-2 depend on heparan sulfate proteoglycans. EMBO J.
718 2021;40:e106765.
719 40. Hötzel I. Deep-time structural evolution of retroviral and filoviral surface envelope proteins. J
720 Virol. 2022;96:e00063-22.

721 41. Rua R, Betsem E, Calattini S, Saib A, Gessain A. Genetic characterization of simian foamy viruses
722 infecting humans. J Virol. 2012;86:13350-9.
723 42. Wagner TC, Bodem J. Sequence errors in foamy virus sequences in the GenBank database:
724 resequencing of the prototypic foamy virus proviral plasmids. Arch Virol. 2016.
725 43. Hutter S, Mullers E, Stanke N, Reh J, Lindemann D. Prototype foamy virus protease activity is
726 essential for intraparticle reverse transcription initiation but not absolutely required for uncoating
727 upon host cell entry. J Virol. 2013;87:3163-76.
728 44. Heinkelein M, Dressler M, Jarmy G, Rammling M, Imrich H, Thurow J, et al. Improved primate
729 foamy virus vectors and packaging constructs. J Virol. 2002;76:3774-83.
730 45. Krey T, d'Alayer J, Kikuti CM, Saulnier A, Damier-Piolle L, Petitpas I, et al. The disulfide bonds in
731 glycoprotein E2 of hepatitis C virus reveal the tertiary organization of the molecule. PLoS Pathog.
732 2010;6:e1000762.
733 46. Bunch TA, Grinblat Y, Goldstein LS. Characterization and use of the Drosophila metallothionein
734 promoter in cultured Drosophila melanogaster cells. Nucl Acids Res. 1988;16:1043-61.
735 47. Backovic M, Krey T. Stable drosophila cell lines: An alternative approach to exogenous protein
736 expression. Meth Mol Biol. 2016;1350:349-58.
737 48. Lambert C, Rua R, Gessain A, Buseyne F. A new sensitive indicator cell line reveals cross-
738 transactivation of the viral LTR by gorilla and chimpanzee simian foamy viruses. Virology.
739 2016;496:219-26.
740 49. Singh H, Ansari HR, Raghava GP. Improved method for linear B-cell epitope prediction using
741 antigen's primary sequence. PLoS One. 2013;8:e62216.
742 50. Larsen JE, Lund O, Nielsen M. Improved method for predicting linear B-cell epitopes.
743 Immunome Res. 2006;2:2.
744 51. Ponomarenko J, Bui HH, Li W, Fusseder N, Bourne PE, Sette A, et al. ElliPro: a new structure-
745 based tool for the prediction of antibody epitopes. BMC Bioinformatics. 2008;9:514.
746 52. Gliniak BC, Kozak SL, Jones RT, Kabat D. Disulfide bonding controls the processing of retroviral
747 envelope glycoproteins. J Biol Chem. 1991;266:22991-7.
748 53. Kelley LA, Mezulis S, Yates CM, Wass MN, Sternberg MJ. The Phyre2 web portal for protein
749 modeling, prediction and analysis. Nat Protoc. 2015;10:845-58.
750 54. Ansari HR, Raghava GP. Identification of conformational B-cell Epitopes in an antigen from its
751 primary sequence. Immunome Res. 2010;6:6.

752

753 # Figure legends

754 ## Fig. 1. Current knowledge of SFV Env and its RBD

755 A. Schematic representation of SFV Env. The precursor Env protein is cleaved by furin-like protease(s)
756 at two sites (vertical bars) to generate LP, SU, and TM. The dark sections highlight the transmembrane
757 regions of LP (H) and TM (MSD), and the fusion peptide (F). The minimal continuous RBD (aa 225-555,
758 blue background) comprises two regions essential for SU binding to cells, RBD1 (aa 225-396) and RBD2
759 (aa 484-555) [13]. The intervening region (aa 397-483), named RBDj, can be deleted without abrogating
760 binding to susceptible cells. Genetic studies on SFV strains circulating in Central Africa have identified
761 two genotypes that differ in the sequence encoding the central part of the SU (SUvar, aa 248-488)
762 domain [11, 12]. SUvar partially overlaps with the RBD and is the exclusive target of nAbs [7]. B. The
763 RBD (aa 218-552) structure from a genotype II gorilla SFV strain is shown as a ribbon (PDB code 8AIC),
764 with SUvar in red and SUcon in grey [14]. Side chains of the glycans are shown and were identified on
765 deglycosylated RBD [14]. Structural elements relevant for the present study are indicated. C. Schematic
766 representation of the two RBD subdomains and their location at the top of Env trimers; the drawing
767 highlights the region involved in trimer assembly [14, 15]. D. RBDj is located at the apex of the RBD
768 upper subdomain; RBD1 forms the second part of the upper subdomain, prolonged in the lower
769 subdomain by an arm wrapping around the stem (RBD2), of which the sequence is conserved.
770 Structural features described in [14] are highlighted on the solvent exposed face of the RBD: the loops
771 mediating trimer interaction (loop 1 is on the internal face and thus not depicted), the conserved
772 glycosylation site (N8), and the HBS. E. The SUvar domain forms the upper RBD subdomain and part of
773 the lower subdomain.

774 ## Fig. 2. The SFV SU block nAbs

775 A. Schematic presentation of the neutralization assay using immunoadhesin as competitor. SU
776 immunoadhesins are chimeric proteins composed of SU, the constant fragment of murine IgG2a, and
777 a double Strep-tag. The SU, RBD, and SUvar are highlighted in the drawing. Plasma samples were

778 diluted to achieve a reduction in the number of FVV-transduced cells by 90%. WT SU compete with Env
779 on FVV for binding by nAbs, resulting in a higher number of FVV-transduced cells; mutations in SU that
780 affect binding by nAbs result in inefficient competition and reduced FVV transduction. Representative
781 images of wells with FVV-transduced cells stained by X-gal are shown. B. The BAK132 (anti-GI) and
782 MEBAK88 (anti-GII) plasma samples were incubated with SU and the mix added to FVVs expressing
783 matched Env before titration. The relative proportion of transduced cells is expressed as the
784 percentage of cells transduced by untreated FVVs (no plasma and no protein), is referred to as the
785 relative infectivity, and is presented as a function of protein concentration. The addition of ^{CI}SU (blue
786 symbols) inhibited the action of nAbs from sample BAK132, as shown by increased CI-PFV Env FVV
787 relative infectivity, whereas ^{GII}SU (red symbols) had no effect. Conversely, ^{GII}SU inhibited the action of
788 nAbs from sample MEBAK88. ^{MLV}SU (grey symbols) had no effect on the plasma antibodies. C. The
789 infectivity of the CI-PFV and GII-K74 Env vectors was quantified in the presence of ^{CI}SU, ^{GII}SU, and ^{MLV}SU;
790 the relative infectivity is presented as a function of protein concentration. D. Schematic representation
791 of a WT SU titration curve, summarized by two parameters, MaxI and IC_{50}. E and F. Thirteen pairs of
792 plasma samples and genotype-matched SU were tested at least five times for their activity against
793 FFVs. The mean and standard error of the mean of the IC_{50} (panel E) and MaxI (panel F) are shown for
794 the CI-PFV Env vectors and anti-GI plasma samples (blue symbols) and the GII-K74 Env vectors and anti-
795 GII plasma samples (red symbols). G. To define neutralizing epitopes, we synthesized SU mutants with
796 four types of alterations in SUvar: mutations, deletion, glycan insertion, and swapping of sequences
797 with the second genotype. H. Schematic representation of titration curves corresponding to SU
798 mutants that lose their capacity to block a fraction of nAbs (mut1, green), block all nAbs with reduced
799 affinity (mut2, orange), or block a fraction of nAbs with reduced affinity (mut 3, pink) or those with no
800 blocking activity (mut4, purple). Two parameters were defined using the curves, MaxI and IC_{50}, and
801 were compared to those obtained with WT SU (panels E and F) to detect significant differences in
802 binding (see Materials and Methods).

803 ## Fig. 3. SFV-specific nAbs recognize glycans on SUvar

804 A. Schematic representation of N-glycosylation sites on the SU. The N7' site (position 374, brown
805 symbol) is absent from CI-PFV but present in zoonotic gorilla SFV and several chimpanzee SFVs [11].
806 The N8 site (position 391, bold stem) is strictly conserved and required for SU expression [23]. The N10
807 site has a genotype-specific location (N411 in GII strains, red symbol; N422 or 423 in GI/CI strains, blue
808 symbol). The glycosylation sites outside SUvar are shown in grey. B. The RBD is shown as a solvent
809 accessible surface, with SUvar in dark grey and SUcon in light grey. The glycans resolved in the SFV RBD
810 X-ray structure are shown as sticks, colored in orange for those for which a deletion mutant was
811 constructed, in black for the N8 and in grey for that located on SUcon; the N5 glycan was poorly
812 resolved and N286 is colored to indicate the localization of its anchor. C and D. To determine whether
813 SFV-specific nAbs target residue glycosylated epitopes, vectors carrying GII-K74 Env were mixed with
814 four genotype-matched plasma samples previously incubated with untreated, kifunensine treated (C),
815 or kifunensine and endo-H treated (D) ^{GII}SU at several concentrations. E. To test whether nAbs target
816 the genotype-specific N10 glycosylation site, the SU in which N10 was removed (^{GII}ΔN10) was
817 incubated with four genotype-matched plasma samples. F. Residues 407-413 were swapped with
818 those from the GI-D468 strain and the resulting ^{GII}swap407 was tested for its ability to block four anti-
819 GII plasma samples. The glycosylation sites located on the SUvar were inactivated one by one (except
820 N8) and tested for their inability to block four GII-specific plasma samples (G to K). ^{GII}ΔN7' was tested
821 against three additional samples to confirm its impact on nAbs (J). For each plasma sample, the IC_{50} is
822 presented as a function of MaxI for untreated and enzyme-treated ^{GII}SU (C and D) or ^{GII}SU and mutants
823 (E to K). The IC_{50} and MaxI values for untreated ^{GII}SU are presented as open symbols and are from the
824 same experiment in which the mutant SU were tested. For the enzyme-treated and mutant SU, the
825 symbols are colored according to the IC_{50} and MaxI thresholds that were used to statistically define
826 significant differences from ^{GII}SU.

827 ## Fig. 4. Most plasma samples contain nAbs that recognize the RBDj domain

828 A. Schematic representation of the SU, with the RBD, the loops, and the inserted glycosylation sites. B.
829 The RBD is shown as a solvent accessible surface with SUvar in dark grey, SUcon in light grey, the side
830 chain from the N8 glycans in dark grey, L2 in orange, L3 in green, L4 in maroon, HBS in black, and the
831 positions of glycosylation site insertions in dark red. To locate SFV-specific nAb epitopes on the upper
832 RBD subdomain, ^{GII}SU and mutants with RBDj deleted (^{GII}ΔRBDj, panel C), deleted loops (^{GII}ΔL2, ^{GII}ΔL3,
833 and ^{GII}ΔL4 in panels D-F), and glycans inserted in putative epitopes (at positions 426, 450, 459, 485, and
834 263 in panels G to K) were tested against at least four plasma samples. Those for which the capacity to
835 block nAbs was the most altered were then tested on additional samples. For each plasma sample, the
836 IC_{50} is presented as a function of MaxI for ^{GII}SU and the mutant SU. The IC_{50} and MaxI values for ^{GII}SU
837 are presented as open symbols and are from the same experiment in which the mutant SU were tested.
838 Symbols are colored according to the IC_{50} and MaxI thresholds used to define statistically significant
839 differences from ^{GII}SU.

840 ## Fig. 5. Epitope disruption by glycan insertion reveals an epitope site on the lower RBD
841 subdomain

842 A. Schematic representation of the SU, with the RBD, loops, HBS, and site of glycan insertion at position
843 351 on SU. B. The RBD is shown as a solvent accessible surface with SUvar in dark grey, SUcon in light
844 grey, HBS in black, and the glycan insertion site in dark red. In the top insert, the 345-353 loop and
845 adjacent helix are presented as ribbons and side chains for GII-K74 (red) and CI-PFV (blue, AlphaFold2-
846 predicted structure). In the bottom insert, the 345-353 loop (red) and adjacent helix are presented as
847 ribbons and side chains for GII-K74, with colored residues indicating the HBS (black), swap333
848 construct (light brown), insertion site at position 349, and two residues on the adjacent helix (green).
849 To locate SFV-specific nAb epitopes on SU functional domains, vectors carrying GII-K74 Env were
850 treated with GII-specific plasma samples previously incubated with the Env ectodomain carrying WT
851 or mutated HBS (^{GII}K342A/R343A in panel C and ^{GII}K356A/R369A in panel D). E. A candidate genotype-

852 specific sequence(Supplementary Table 1) was disrupted by inserting glycan in the SU at position 351 and
853 tested for its capacity to block nAbs. F to K. Five mutant SU were tested to characterize the epitopic
854 region in the 345-353 loop. All mutants were tested against at least four plasma samples. Those for
855 which the capacity to block nAbs was the most altered were then tested on additional samples. For
856 each plasma sample, the IC_{50} is presented as a function of MaxI for ^{GII}SU and the mutant SUs. The IC_{50}
857 and MaxI values of ^{GII}SU are presented as open symbols and are those from the same experiment in
858 which the mutants were tested. Symbols are colored according to the IC_{50} and MaxI thresholds used
859 to statistically define significant differences from ^{GII}SU. We applied the same threshold values for the
860 analyses of the Env ectodomain, which had the same inhibitory activity as ^{GII}SU (Supplementary Fig. 2).
861 ^{GII}swap333 was tested twice at three concentrations and showed similar blocking capacity as ^{GII}SU; the
862 IC_{50} values were arbitrarily set to the same level as those of ^{GII}SU (see Materials and Methods).

863 Fig. 6. The 345-353 loop is targeted by nAbs at the surface of viral vector particles.

864 A. Three batches of FVVs carrying Env with ^{GII}SU or ^{GII}SUswap345 were produced. The concentration of
865 vector particles was quantified by RT-qPCR amplification of the *bgal* transgene. B. FVV infectious titers
866 were quantified on BHK-21 cells. C. FVVs carrying WT and mutated Env were incubated with HT1080
867 cells at 10 or 100 particles/cells on ice for 1 h before washing and quantification of *bgal* mRNA
868 incorporation in the vector particles and the *gapdh* gene of susceptible cells. The levels of *bgal* and
869 cellular *gapdh* mRNA were quantified by RT-qPCR; the ΔΔCt method was used to calculate the relative
870 number of FVV particles bound to cells. The dotted lines in panels A to C represent the quantification
871 threshold and the black lines the mean values from the three FVV batches. The infectious titers,
872 particle concentration, and levels of bound particles from FVVs carrying mutant or WT SU were
873 compared using the paired t test and all p values were > 0.05. D to J. Neutralization assays were carried
874 out by transducing BHK-21 cells with SFV vectors carrying WT (plain symbols) or swap345 (open
875 symbols) GII Env. Vectors were previously incubated with 10 serial dilutions of human plasma samples;
876 the lowest dilution ranged between 1:20 or 1:160 according to the donors' neutralization titers [7].
877 Assays were performed twice in triplicate and the results from one experiment are shown. Cells were

878 transduced with untreated FFV to provide the reference value. Relative infectivity was calculated for
879 wells treated with plasma samples and is expressed as the percentage of the reference value. Relative
880 infectivity (mean, SEM) is presented as a function of the plasma dilution. Arrows indicate neutralization
881 titers against vectors carrying WT (plain line) and swap345 (broken line) GII Env. Plasma samples are
882 the same as those presented in Fig. 3 to 5: D, BAD447; E, BAD551; F, BAK55; G, BAK133; H, BAK228; I,
883 BAK232; and J, MEBAK88.

884 Fig. 7. GI and GII-specific nAbs target different epitopes

885 CI SU with mutations matching the most informative GII SU mutations were tested for their capacity
886 to block nAbs from GI-specific plasma samples. A, Kifunensin-treated ^{CI}SU; B, Kifunensin and endoH-
887 treated ^{CI}SU; C, ^{CI}ΔN10; D, $^{CI}350_{glyc}$; E, ^{CI}ΔRBDj; F, ^{CI}ΔL2; G, ^{CI}ΔL3; H, ^{CI}ΔL4; I, $^{CI}463_{glyc}$; J, ^{GII}swapRBDj; K,
888 ^{GII}SU; L, ^{CI}swapL3. All mutants were tested against four plasma samples. Those for which the capacity
889 to block nAbs was the most altered were then tested on additional samples. For each plasma sample,
890 the IC_{50} is presented as a function of MaxI for the ^{CI}SU and mutant SU. The IC_{50} and MaxI values of ^{CI}SU
891 are presented as open symbols and are those from the same experiment in which the mutant SU were
892 tested. For mutant SU, the symbols are colored according to the IC_{50} and MaxI thresholds used to
893 statistically define significant differences from ^{CI}SU. The red lines correspond to data obtained with GII-
894 specific plasma samples against equivalent constructs (Panels 3C, 3D, 3E, 5F, 4C, 4D, 4E, 4F, and 4I
895 match panels 7A to 7H, respectively).

896 Fig. 8. Plasma antibodies do not bind to peptides covering the loops from the upper RBD
897 subdomain

898 Twelve plasma samples from African hunters (Supplementary Table 4) were tested for binding to peptides
899 overlapping loops located in the upper subdomain of the RBD (Supplementary Table 5). Plasma samples
900 from four uninfected (grey symbols), four GI-infected (blue symbols), and four GII-infected (red
901 symbols) individuals were tested. The CMV and SFV Env6 peptides were used as positive controls and
902 the SFV Env5 peptide as a negative control [24]. The peptide diluent was used as the negative control

903 and antibody binding to peptides is expressed as the difference in OD ($\Delta_{OD} = OD_{test} - OD_{control}$). The
904 responses are presented as Δ_{OD} (y-axis) for each peptide (x-axis).

905 Fig. 9. nAbs target epitopic regions involved in SU binding to susceptible cells or required
906 for viral infectivity

907 A. HT1080 cells were incubated with the panel of tested immunadhesins (Fig. 3 to 7). Cell-bound SU
908 were detected by staining with a fluorescently labeled antibody targeting the murine IgG Fc fragment.
909 Stained cells were analyzed on a flow cell cytometer. Supplementary Fig. 8 presents the gating strategy
910 and normalization of the results to the levels of bound WT SU (^{GII}SU and ^{CI}SU). Binding levels of GII
911 mutants are presented by (red symbols). CI mutants (blue symbols) are presented side-by-side with
912 the corresponding and related GII mutants, with a colored background. Mutated HBS shows reduced
913 binding to susceptible cells, as shown in [14].

914 Fig. 10. Human plasma samples contain nAbs targeting a variable number of epitopic
915 regions

916 A. In the present study, we identified three epitopic sites on SUvar: the RBD apex, the N8 region, and
917 the 345-353 loop. The schematic summary highlights L2, L3, and L4, the conserved N8 and adjacent
918 N7' glycosylation site, and the 345-353 loop (lines ending with a dot). Glycans inserted in predicted
919 epitopes revealed additional antigenic sites (lines ending with a triangle). B and C. The results from
920 competition experiments are summarized for each plasma sample and for the mutant SU from the
921 most highly targeted regions (apex, N8 region, and the 345-353 loop). Four outcomes are presented:
922 same recognition as WT SU (green), recognition with reduced affinity (i.e., increased IC_{50}, orange
923 vertical shading), blocking a smaller fraction of nAbs than WT SU (i.e., reduced MaxI, orange
924 horizontal shading), or having both effects (orange). Black squares indicate the major epitopic
925 regions of the GII- and GI-specific samples (panels B and C, respectively). Within each epitopic region
926 defined by several mutant SU, nAb specificity varied between individuals.

927 Fig. 1. Current knowledge of SFV Env and its RBD

928

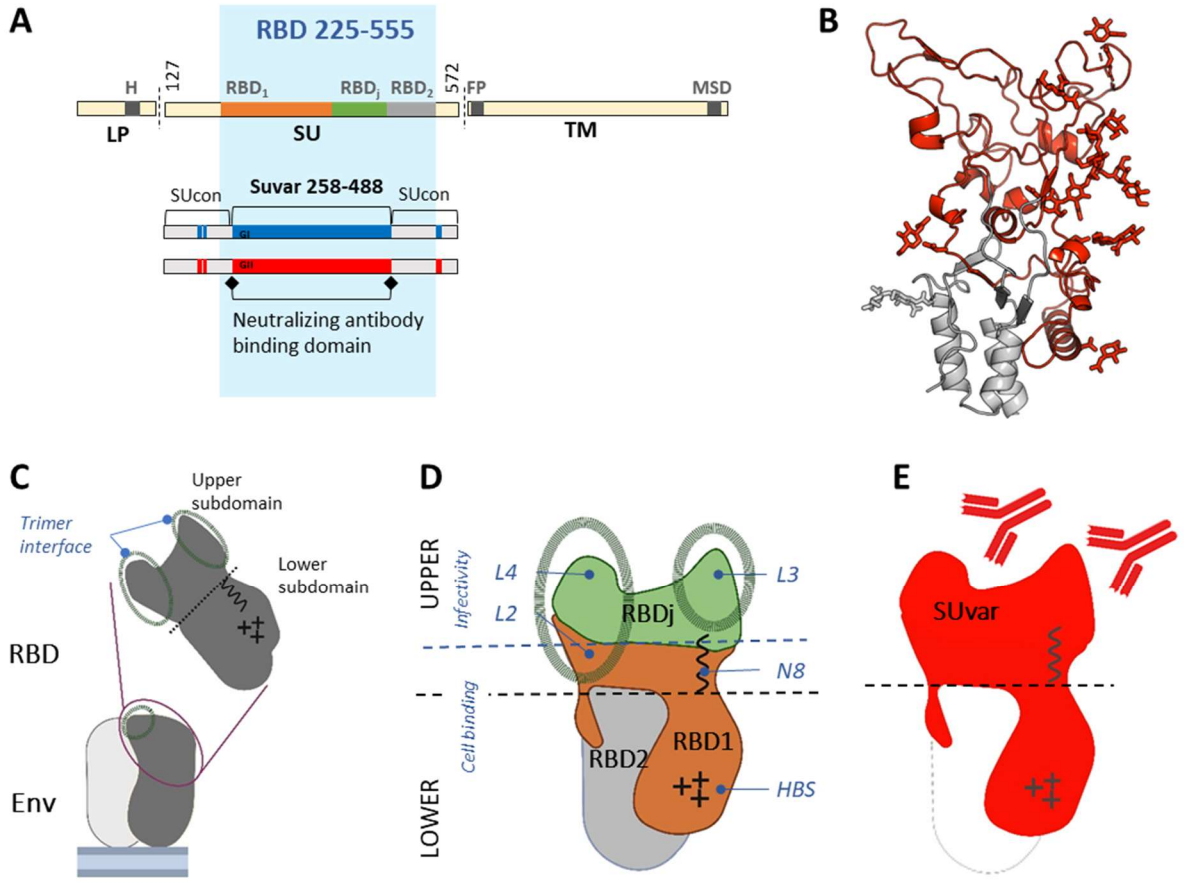

929

930

931 Fig. 2. The SFV SU blocks nAbs

932

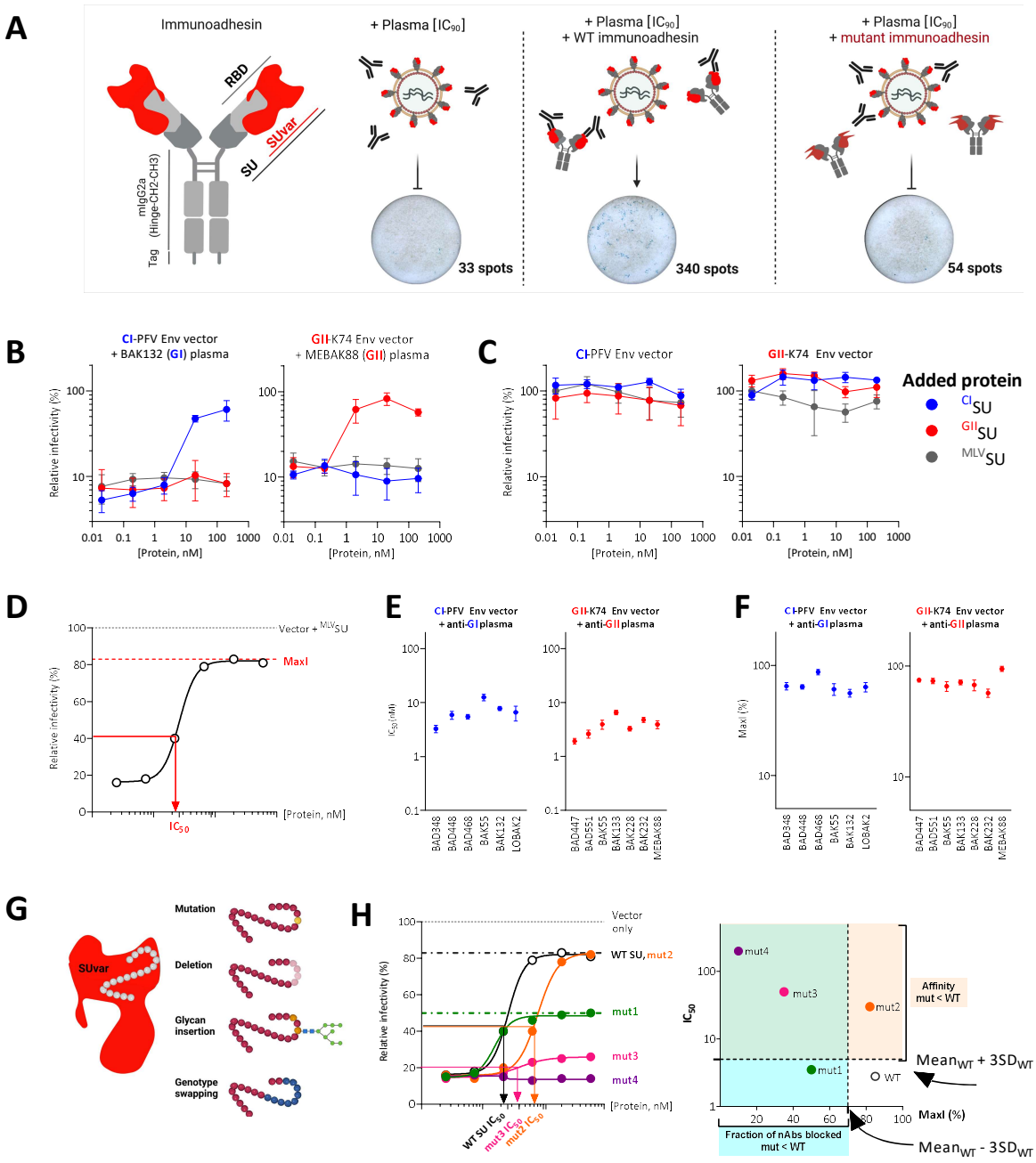

933

934

935 Fig. 3. SFV-specific nAbs recognize glycans on SUvar

936

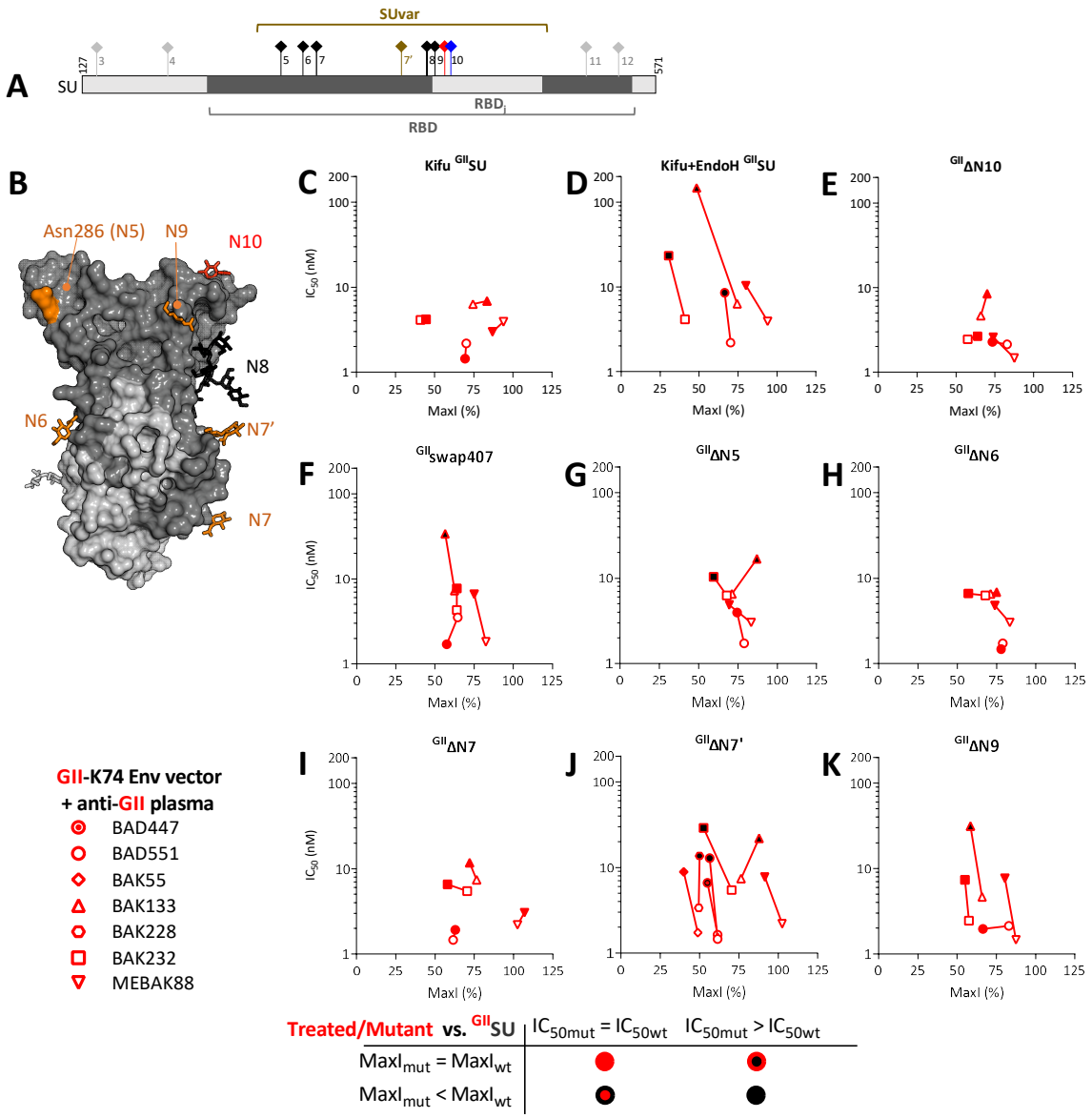

937

Fig. 4. Most plasma samples contain nAbs that recognize the RBDj domain

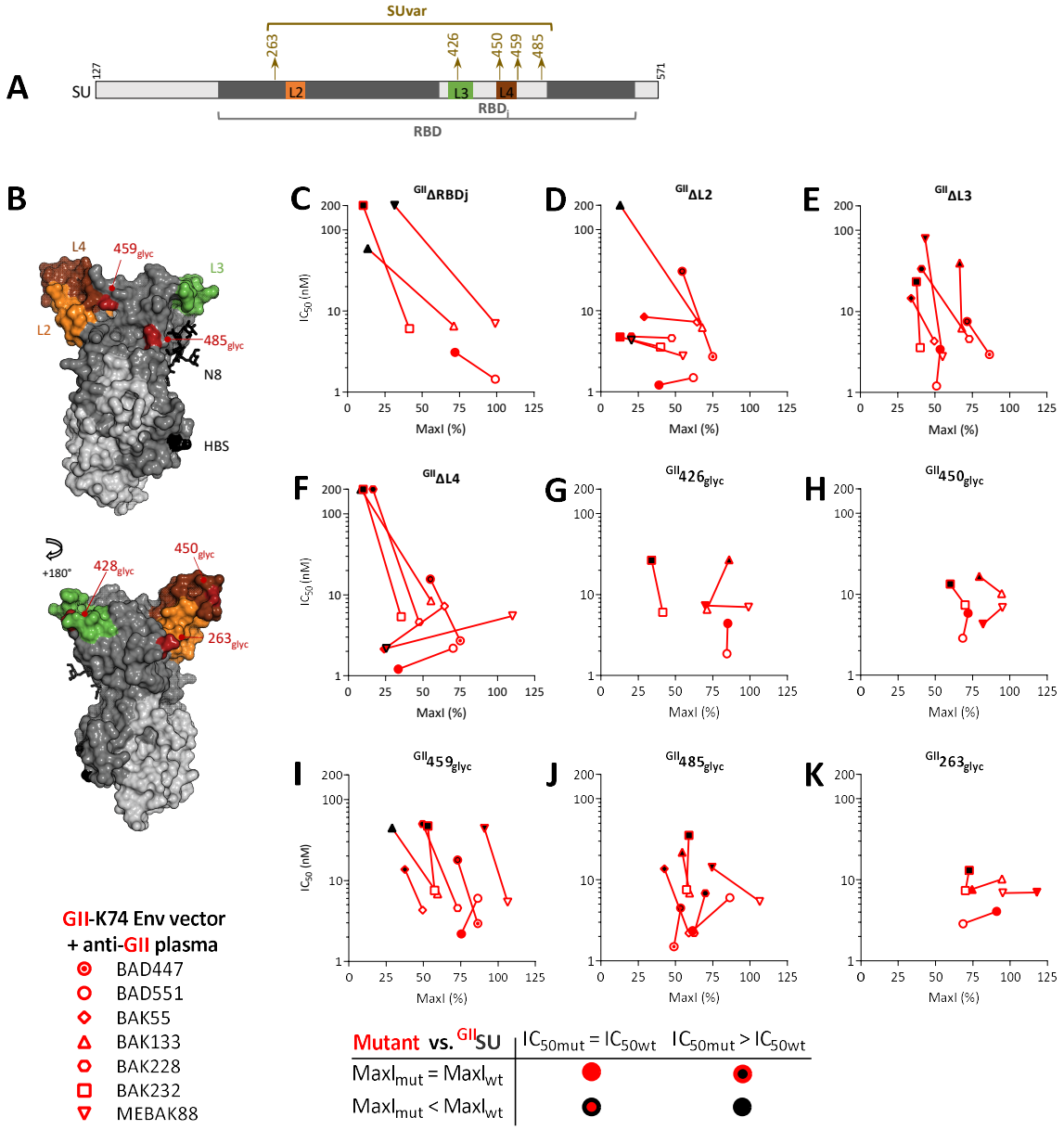

Fig. 5. Epitope disruption by glycan insertion reveals additional nAb recognition sites

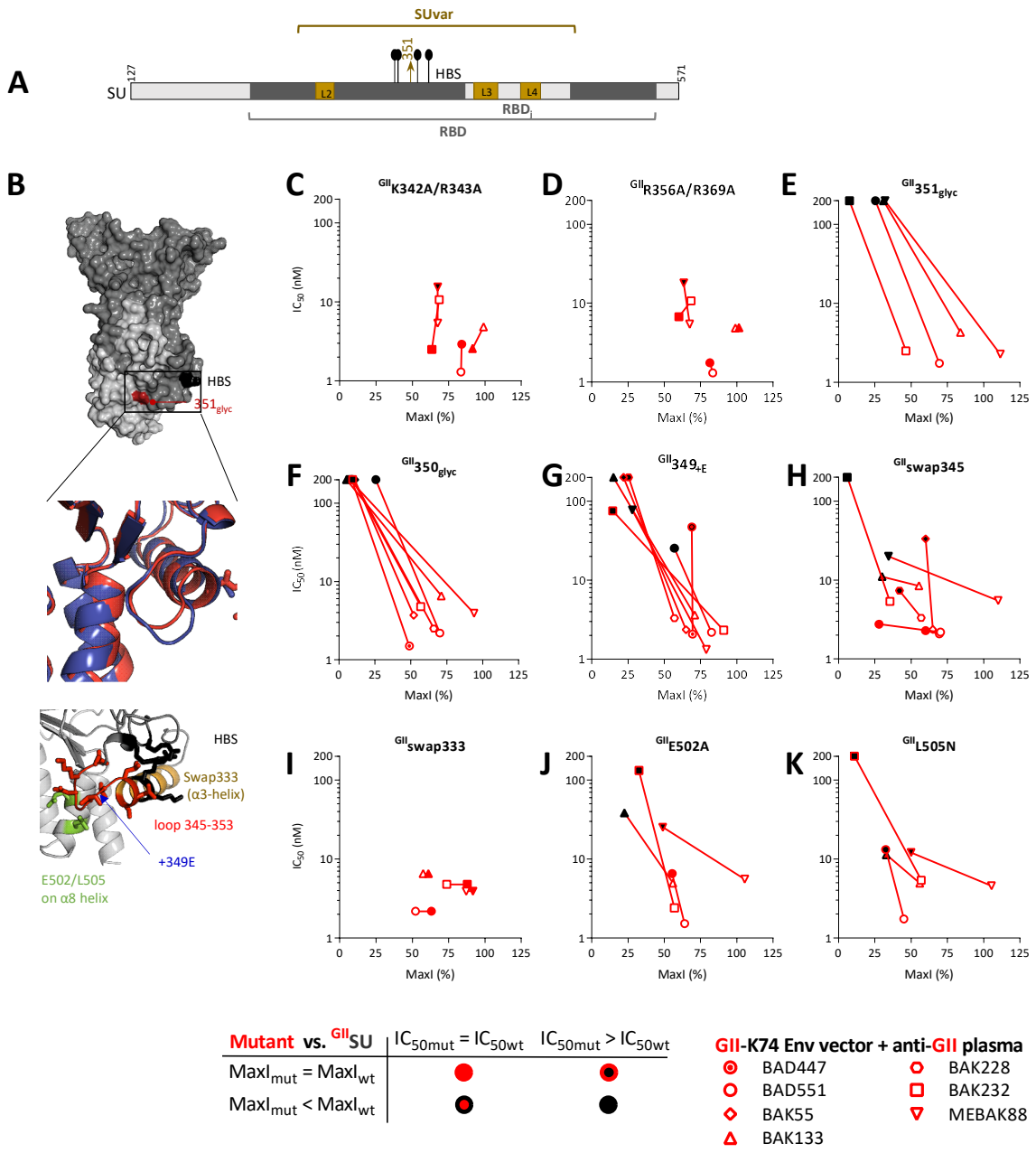

Fig. 6. The 345-353 loop is targeted by nAbs at the surface of viral vector particles.

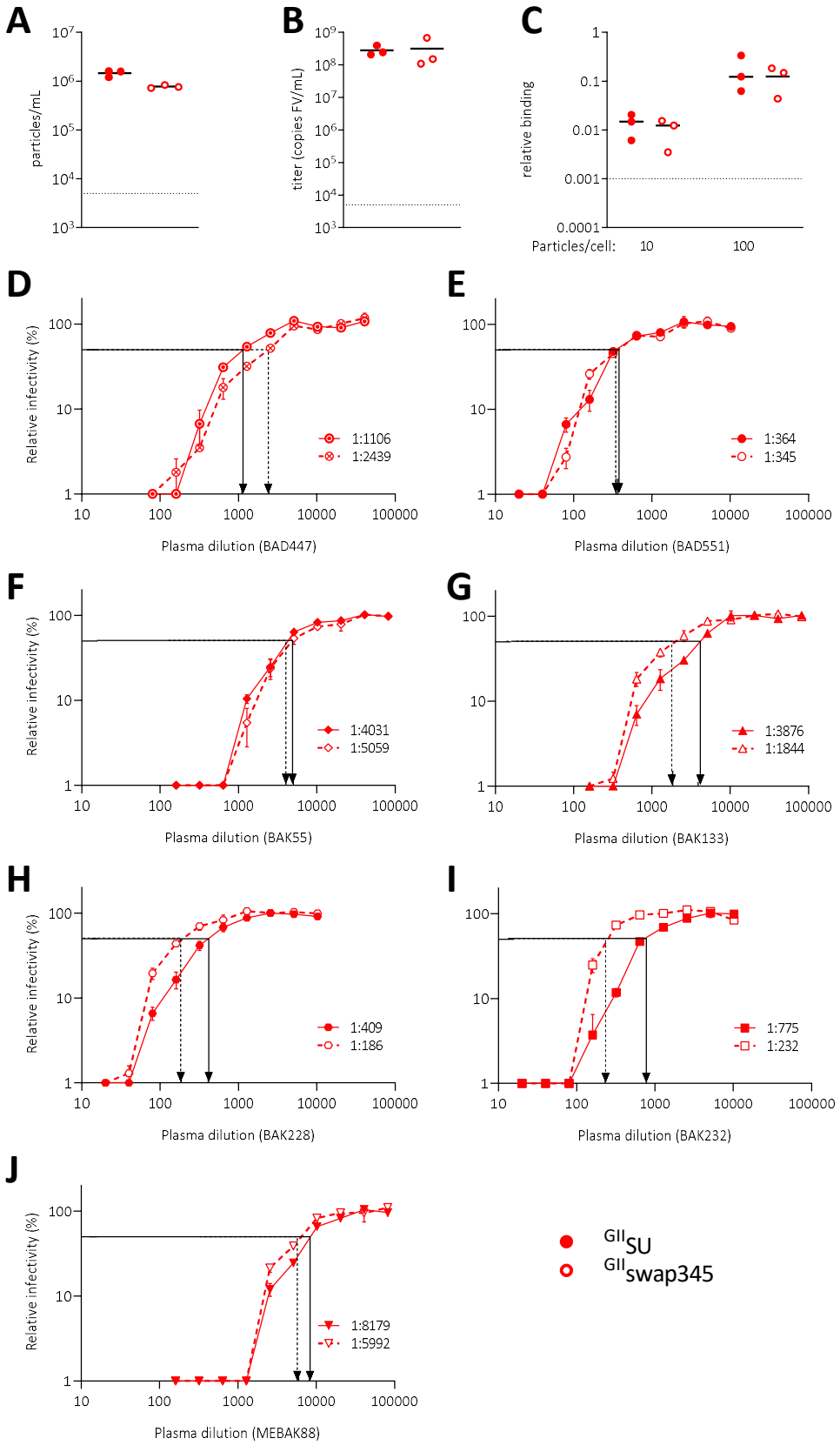

Fig. 7. GI and GII-specific nAbs target different epitopes

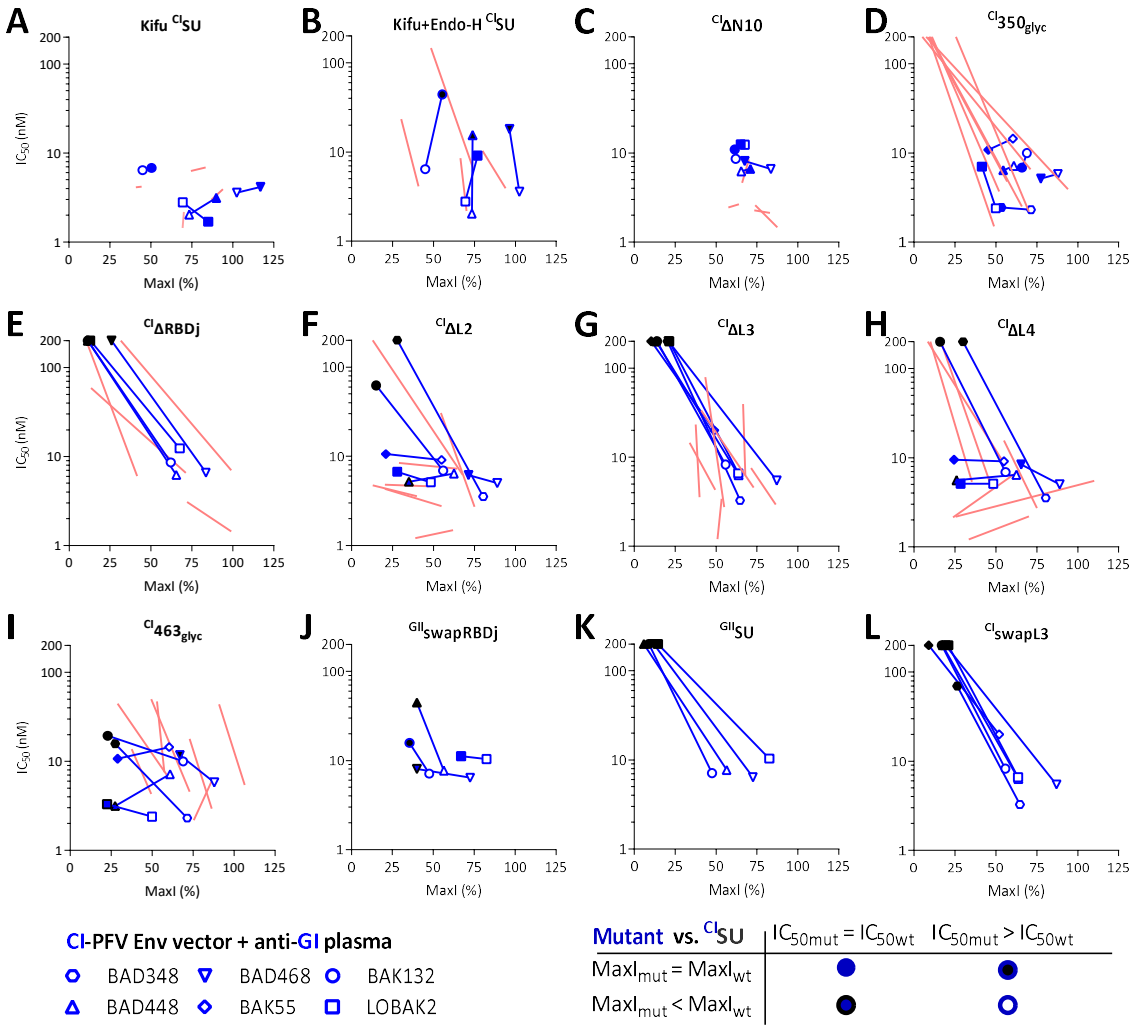

Fig. 8. Plasma antibodies do not bind to peptides covering the loops from the upper RBD subdomain

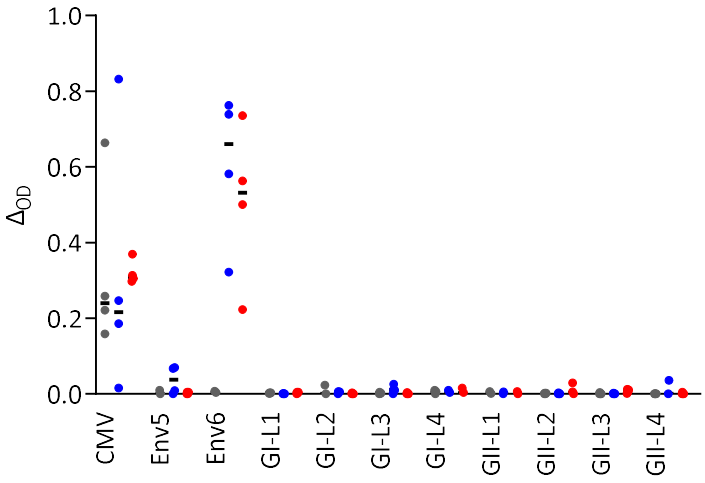

Fig. 9. nAbs target epitopic regions involved in SU binding to susceptible cells or required for viral infectivity

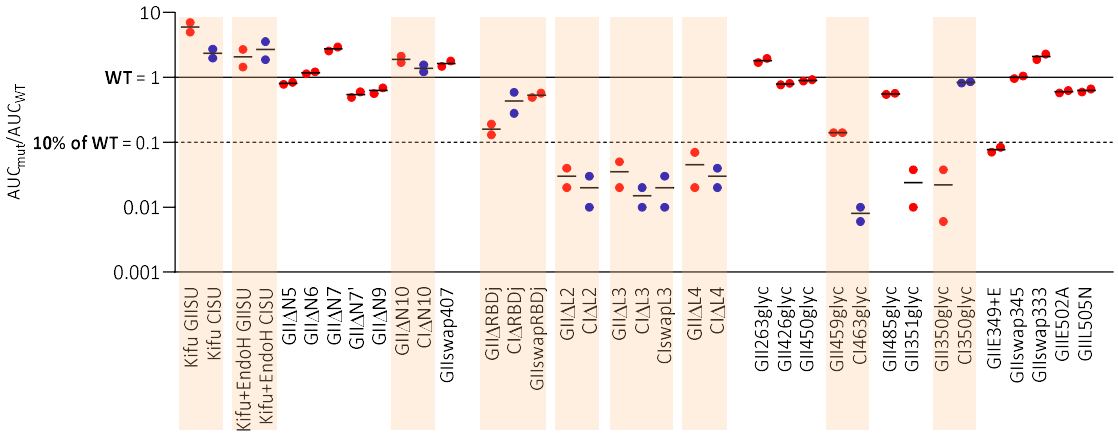
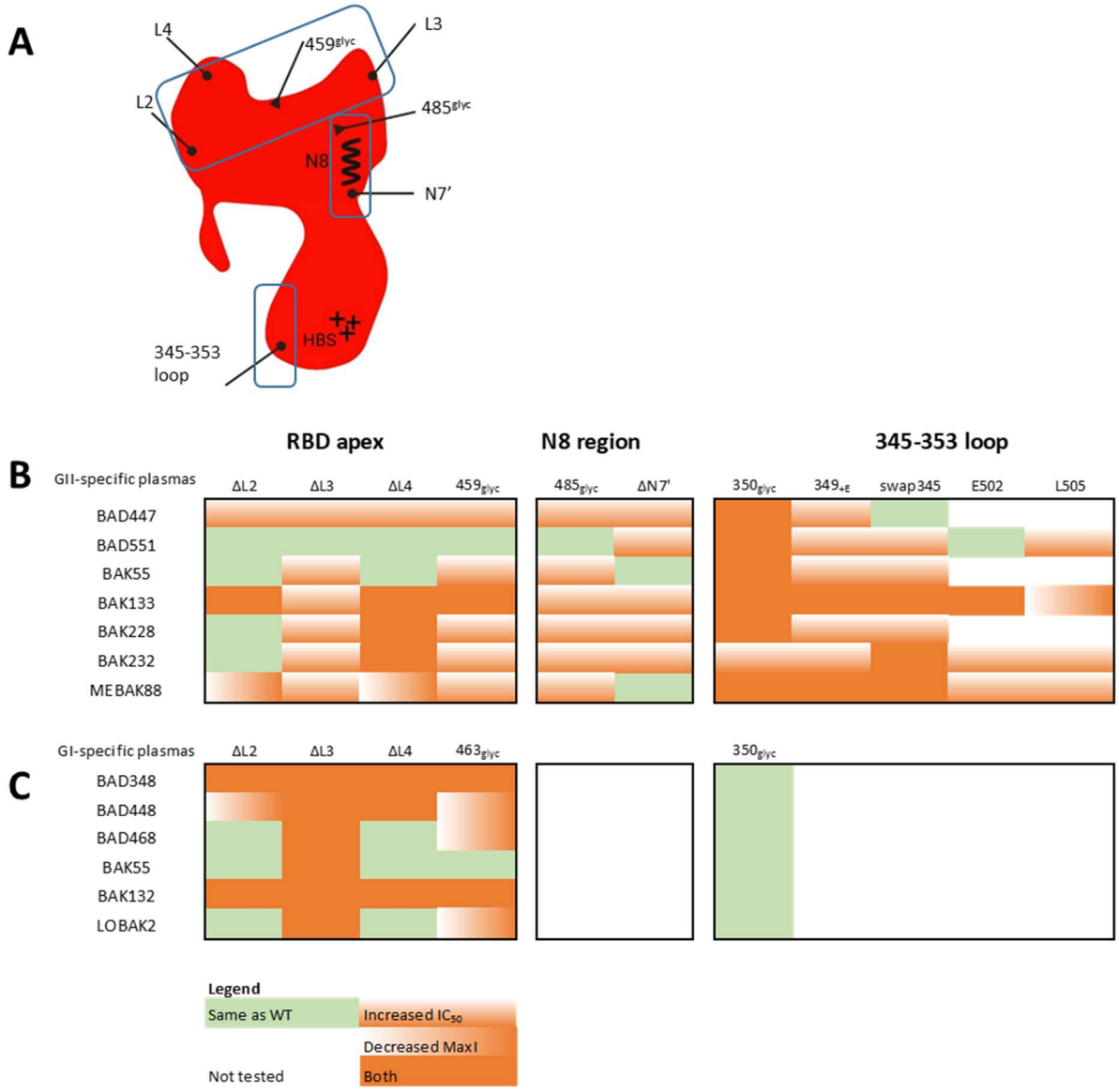
Fig. 10. Human plasma samples contain nAbs targeting a variable number of epitopic regions